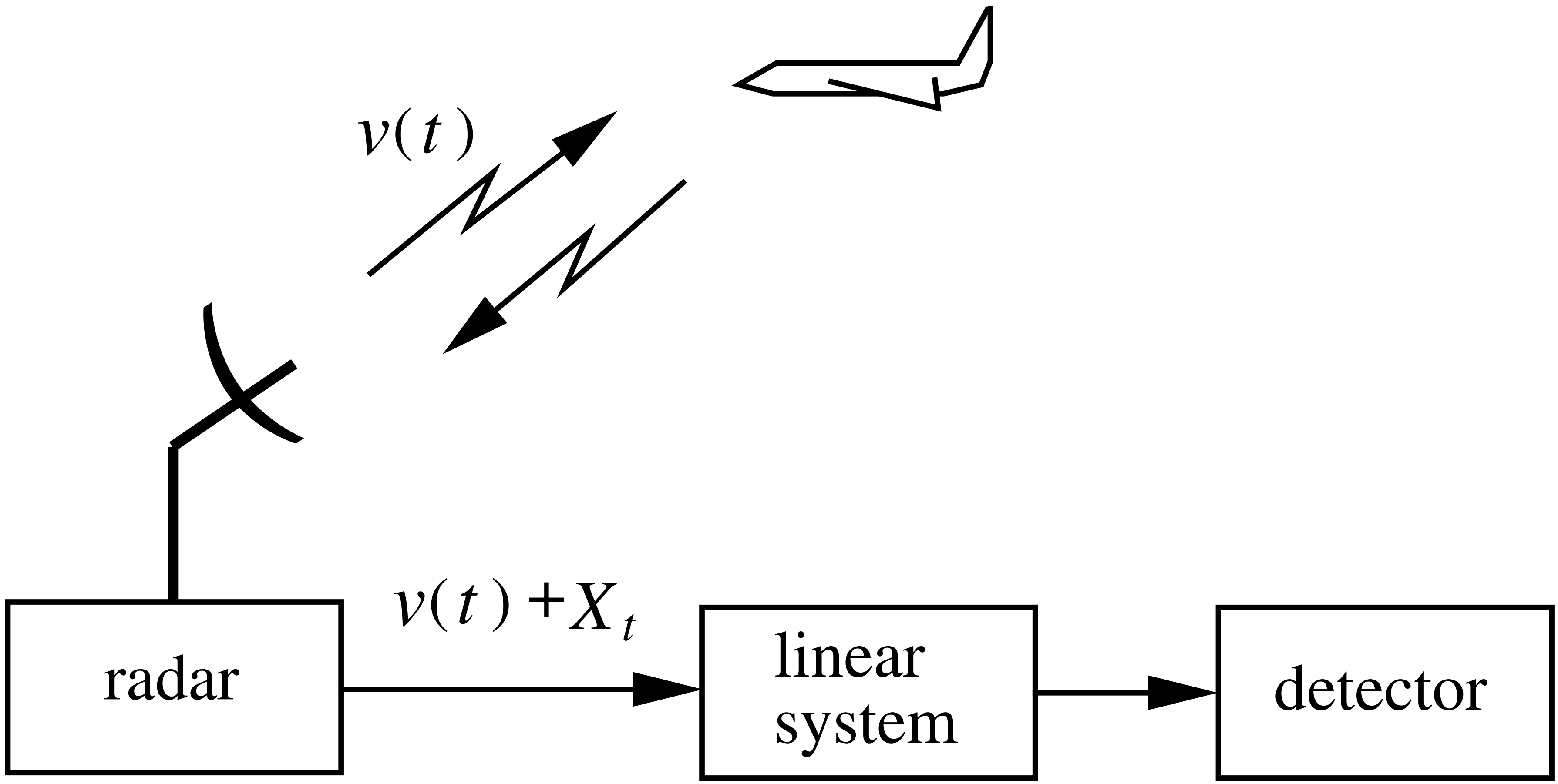

***Figure* 1.1.** Block diagram of radar detection system.

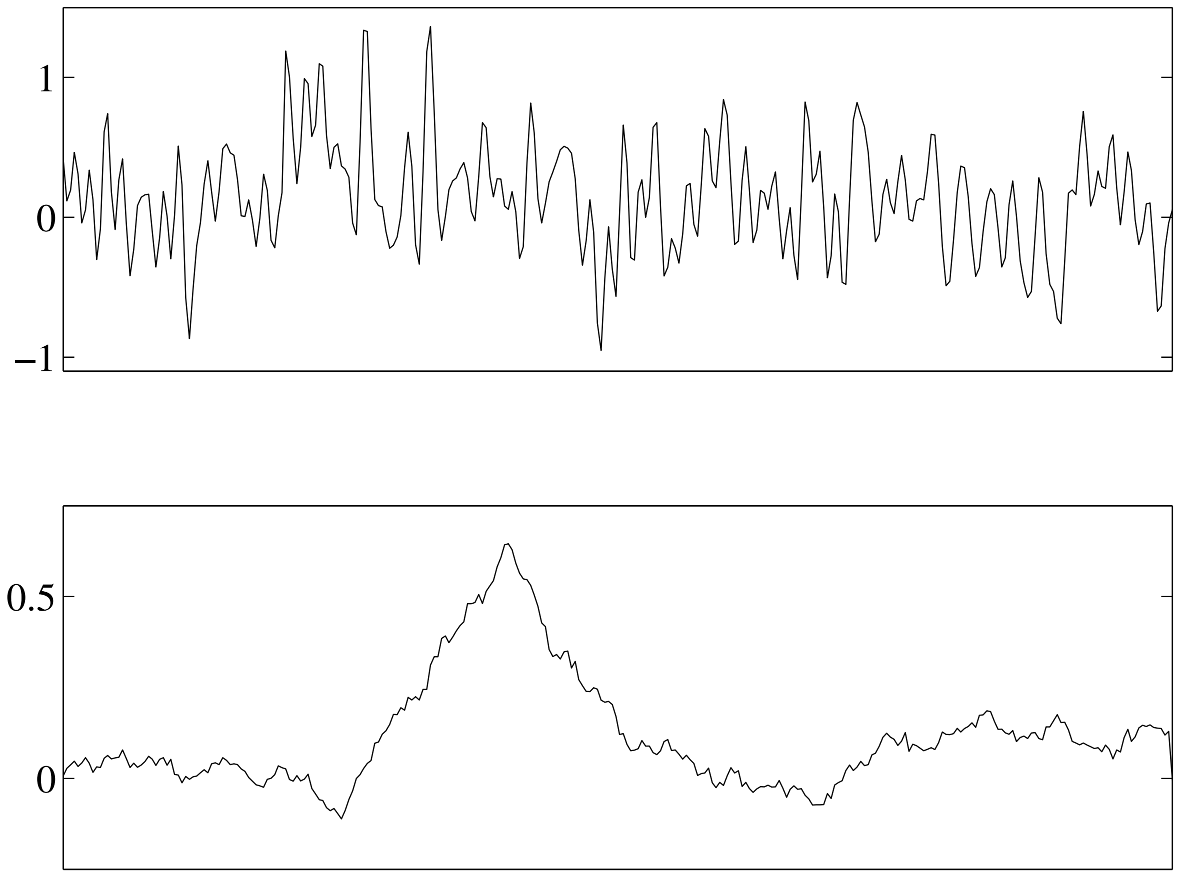

***Figure* 1.2.** Matched filter input (top) in which the signal is hidden by noise. Matched filter output (bottom) in which the signal presence is obvious.

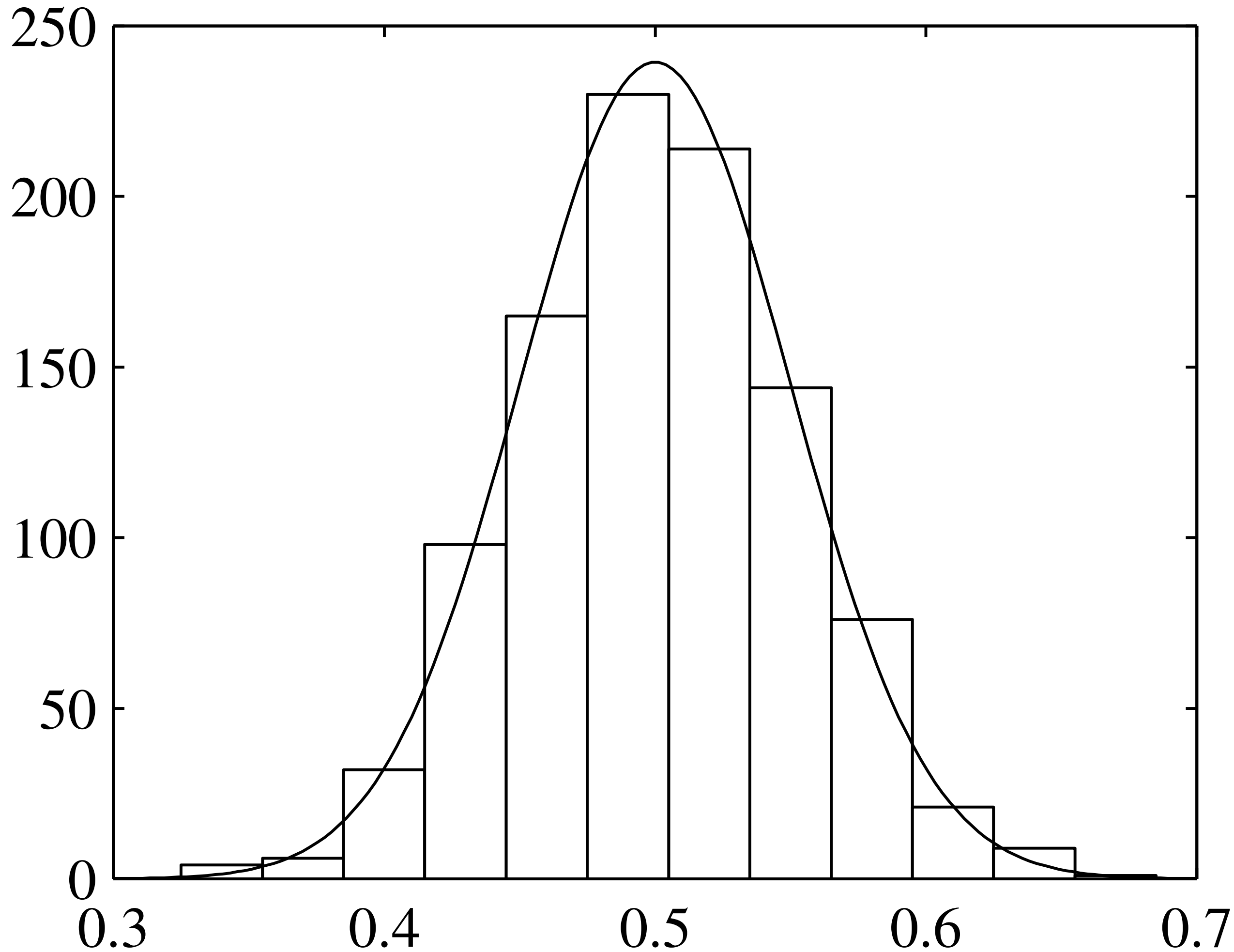

***Figure* 1.4.** Histogram of Example 1.2 with overlay of a Gaussian density.

***Example* 1.2.** We performed the experiment with outcomes $S_0, \ldots, S_{100}$ 1000 times and counted the number of occurrences of each outcome. All trials produced between 33 and 68 heads. Rather than list $N_{1000}(S_k)$ for the remaining values of k, we summarize as follows:

$$\begin{aligned}
N_{1000}(S_{33}) + N_{1000}(S_{34}) + N_{1000}(S_{35}) &= 4 \\
N_{1000}(S_{36}) + N_{1000}(S_{37}) + N_{1000}(S_{38}) &= 6 \\
N_{1000}(S_{39}) + N_{1000}(S_{40}) + N_{1000}(S_{41}) &= 32 \\
N_{1000}(S_{42}) + N_{1000}(S_{43}) + N_{1000}(S_{44}) &= 98 \\
N_{1000}(S_{45}) + N_{1000}(S_{46}) + N_{1000}(S_{47}) &= 165 \\
N_{1000}(S_{48}) + N_{1000}(S_{49}) + N_{1000}(S_{50}) &= 230 \\
N_{1000}(S_{51}) + N_{1000}(S_{52}) + N_{1000}(S_{53}) &= 214 \\
N_{1000}(S_{54}) + N_{1000}(S_{55}) + N_{1000}(S_{56}) &= 144 \\
N_{1000}(S_{57}) + N_{1000}(S_{58}) + N_{1000}(S_{59}) &= 76 \\
N_{1000}(S_{60}) + N_{1000}(S_{61}) + N_{1000}(S_{62}) &= 21 \\
N_{1000}(S_{63}) + N_{1000}(S_{64}) + N_{1000}(S_{65}) &= 9 \\
N_{1000}(S_{66}) + N_{1000}(S_{67}) + N_{1000}(S_{68}) &= 1.
\end{aligned}$$

This summary is illustrated in the histogram shown in Figure 1.4. (The bars are centered over values of the form $k/100$; e.g., the bar of height 230 is centered over 0.49.)

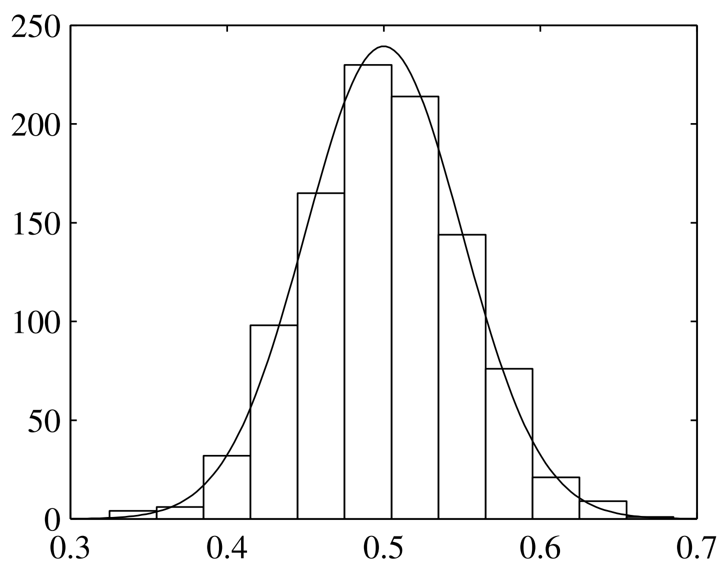

***Figure* 1.4.** Histogram of Example 1.2 with overlay of a Gaussian density.

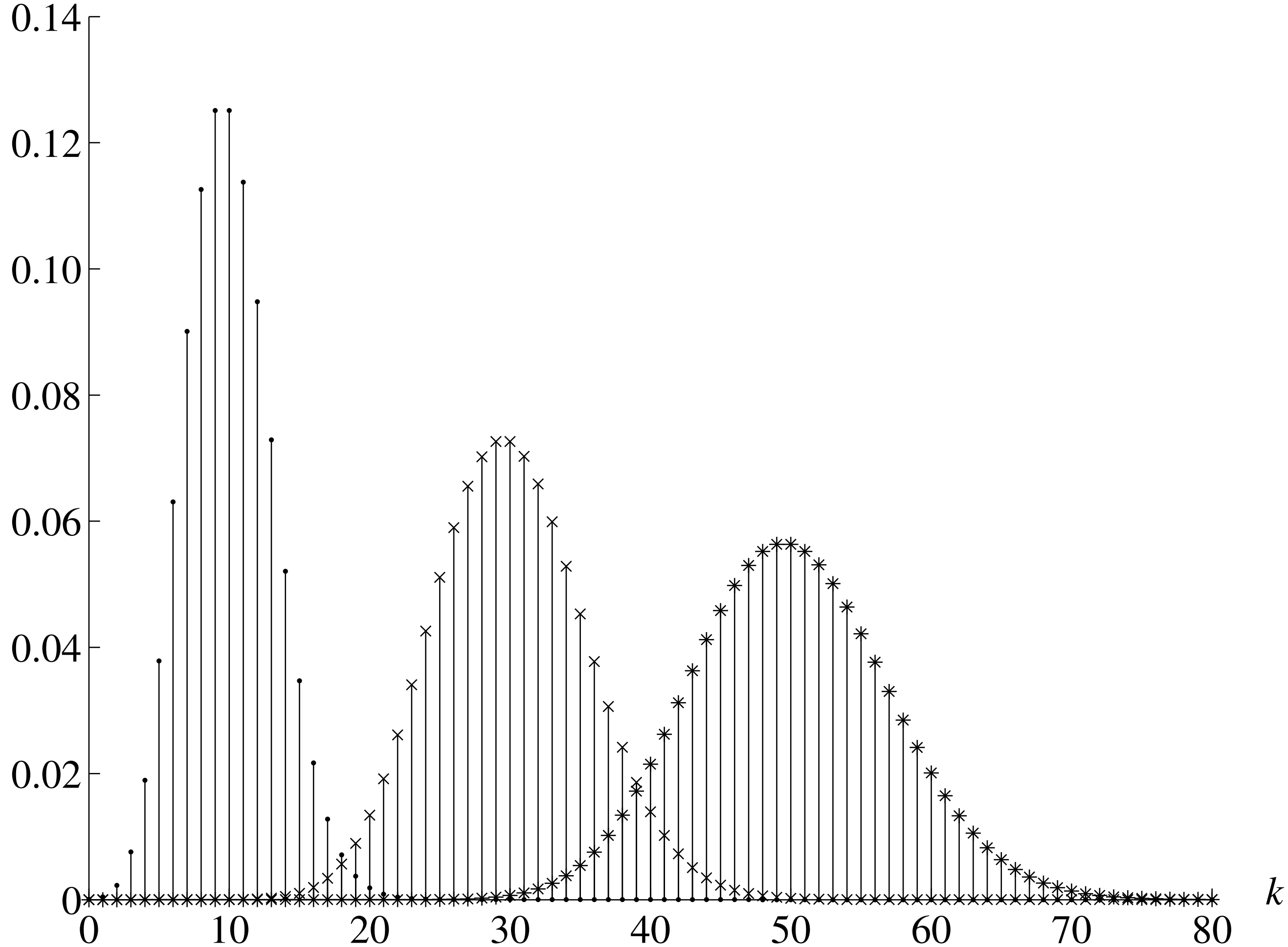

***Figure* 2.5.** The Poisson(λ) pmf $p_X(k) = \lambda^k e^{-\lambda}/k!$ for $\lambda = 10, 30$, and 50 from left to right, respectively.

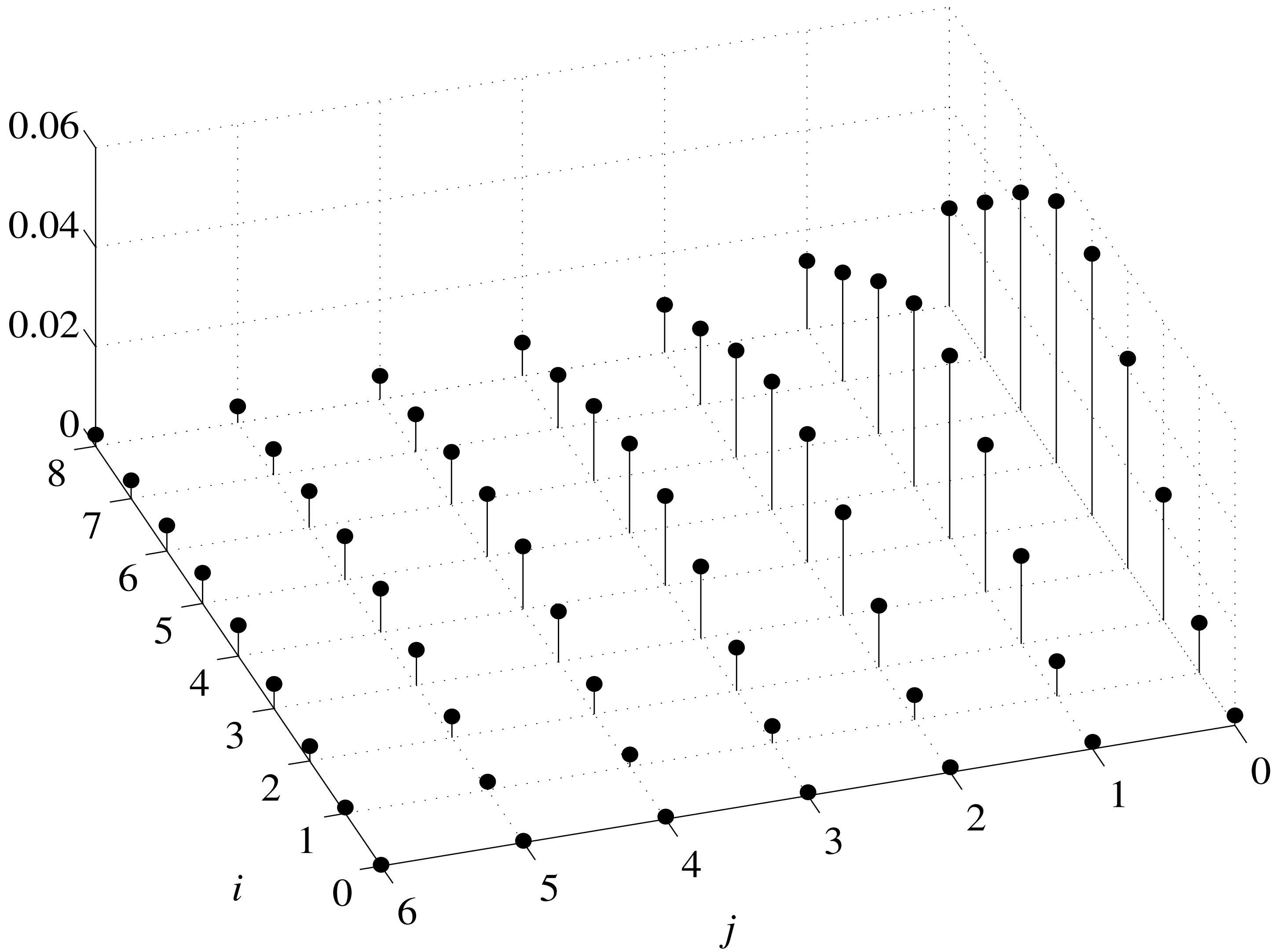

***Figure* 2.8.** Sketch of bivariate probability mass function $p_{XY}(i, j)$.

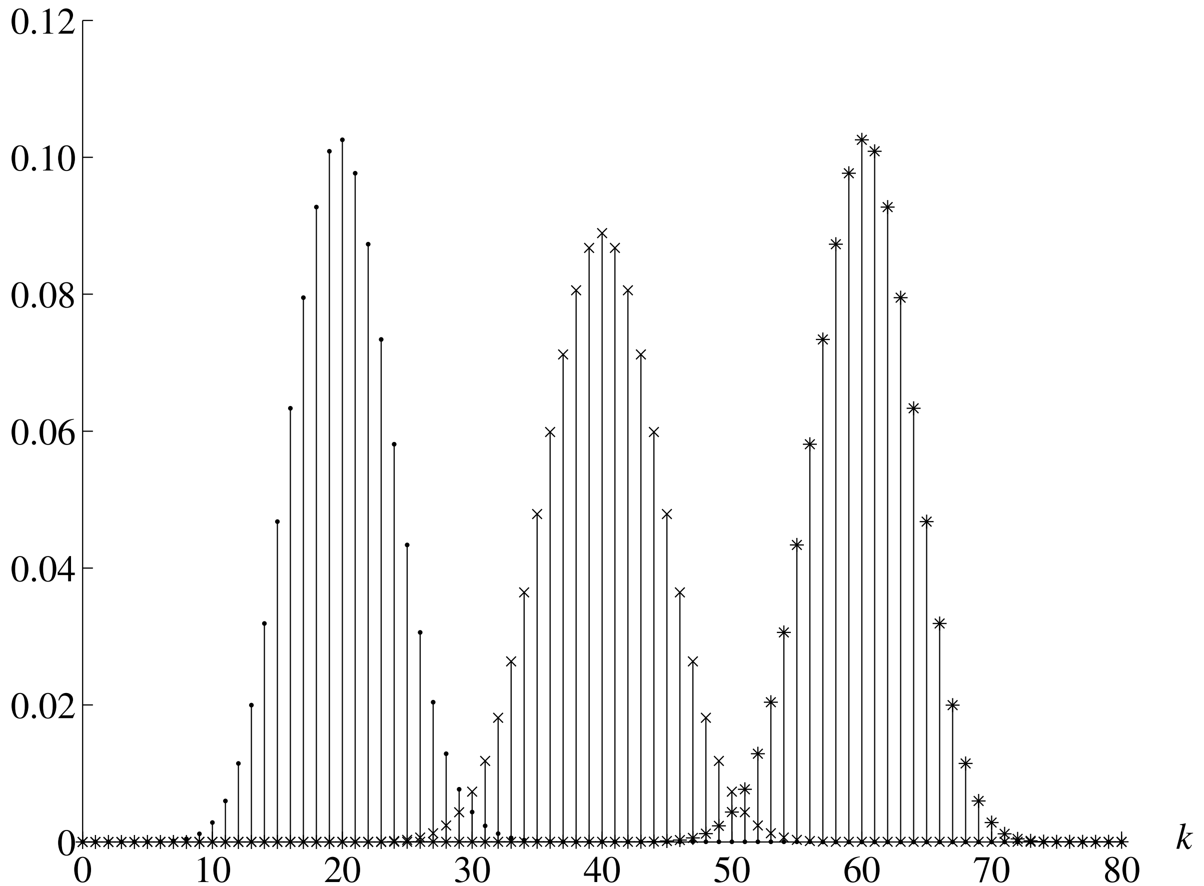

***Figure* 3.1.** The binomial(n,p) pmf $p_Y(k) = \binom{n}{k} p^k (1-p)^{n-k}$ for $n = 80$ and $p = 0.25, 0.5$, and 0.75 from left to right, respectively.

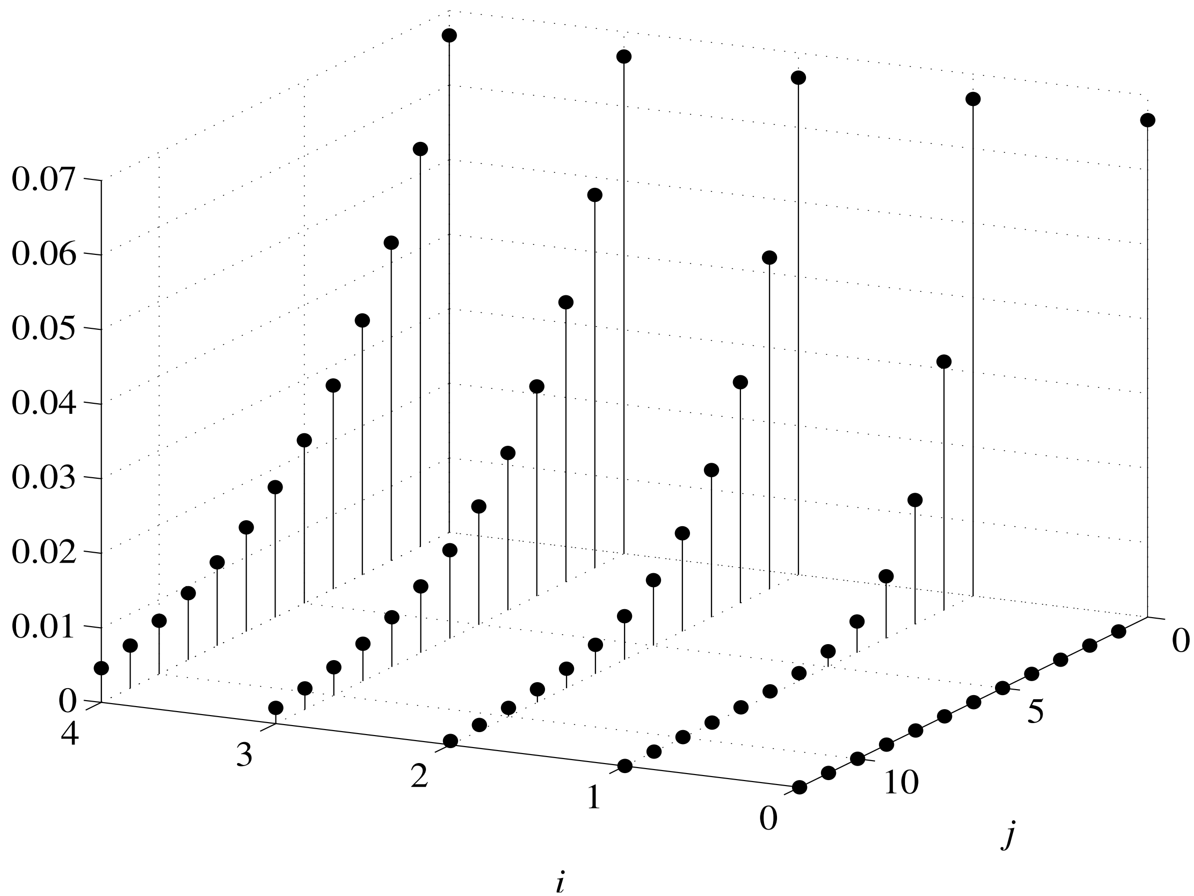

***Figure* 3.3.** Sketch of bivariate probability mass function $p_{XY}(i,j)$ of Example 3.10 with $n=5$. For fixed i, $p_{XY}(i,j)$ as a function of j is proportional to $p_{Y|X}(j|i)$, which is geometric$_0(i/(i+1))$. The special case $i=0$ results in $p_{Y|X}(j|0) \sim$ geometric$_0(0)$, which corresponds to a constant random variable that takes the value $j=0$ with probability one.

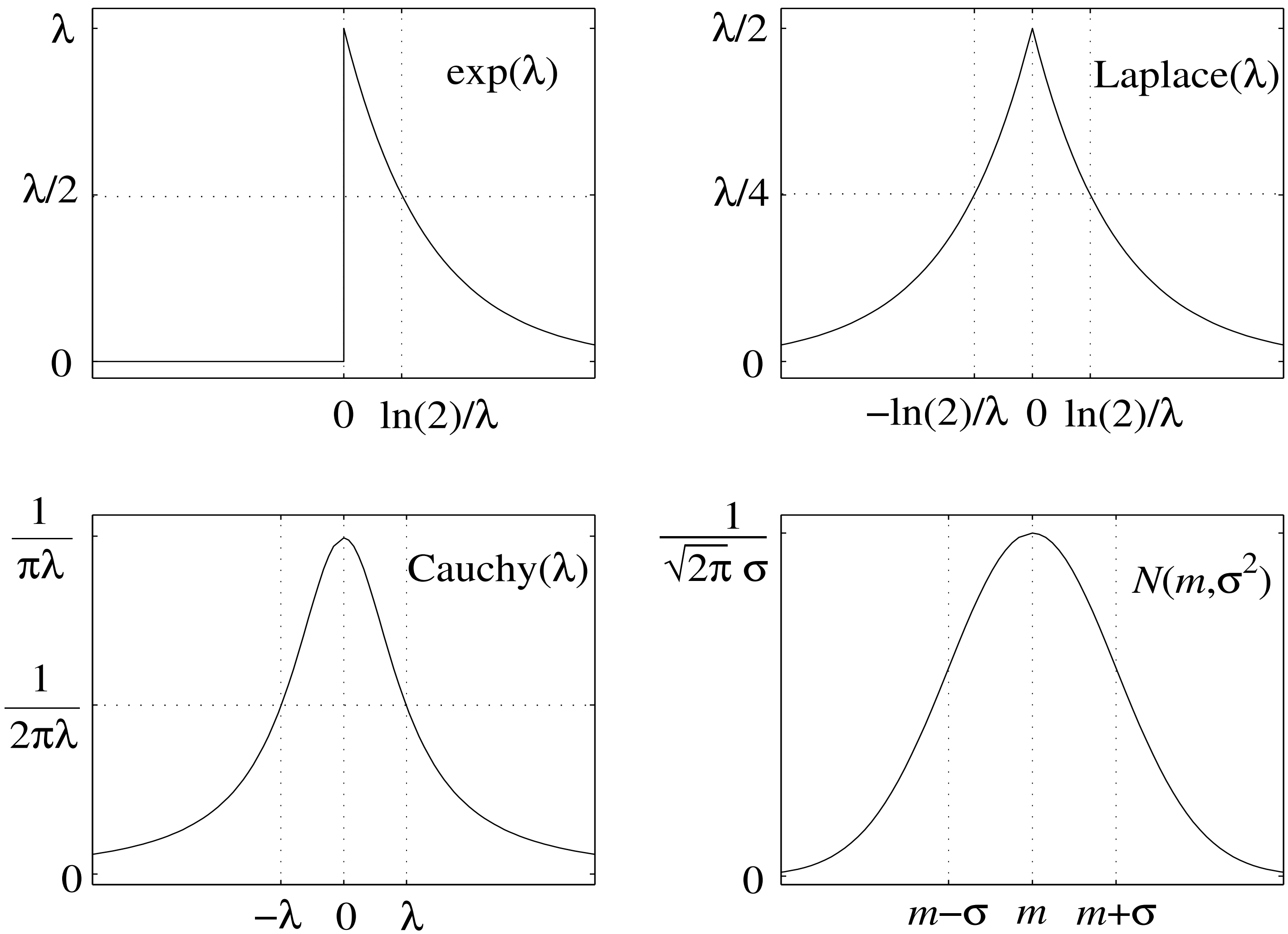

***Figure* 4.3.** Several common density functions.

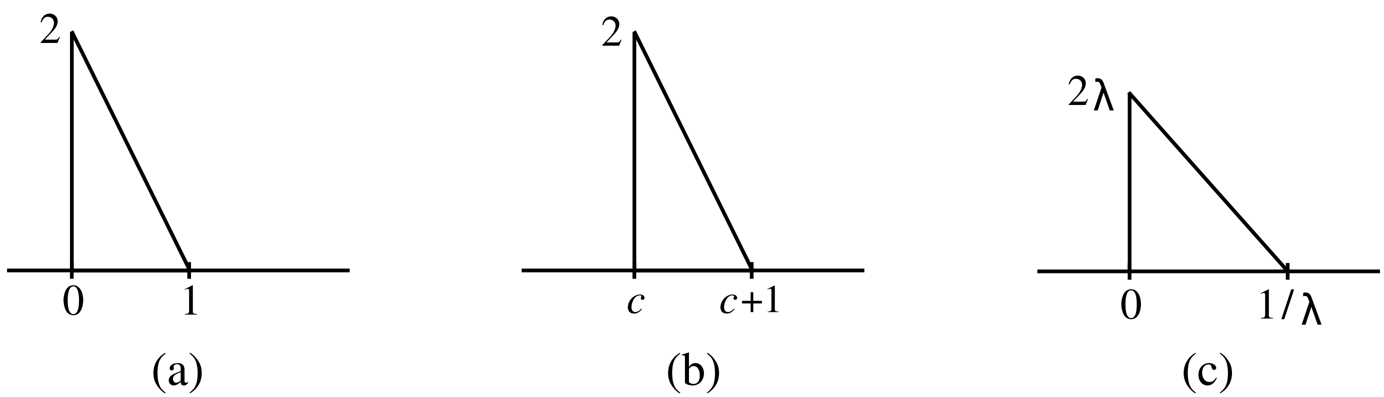

Figure **4.6.** (a) Triangular density $f(x)$. (b) Shifted density $f(x-c)$. (c) Scaled density $\lambda f(\lambda x)$ shown for $0 < \lambda < 1$.

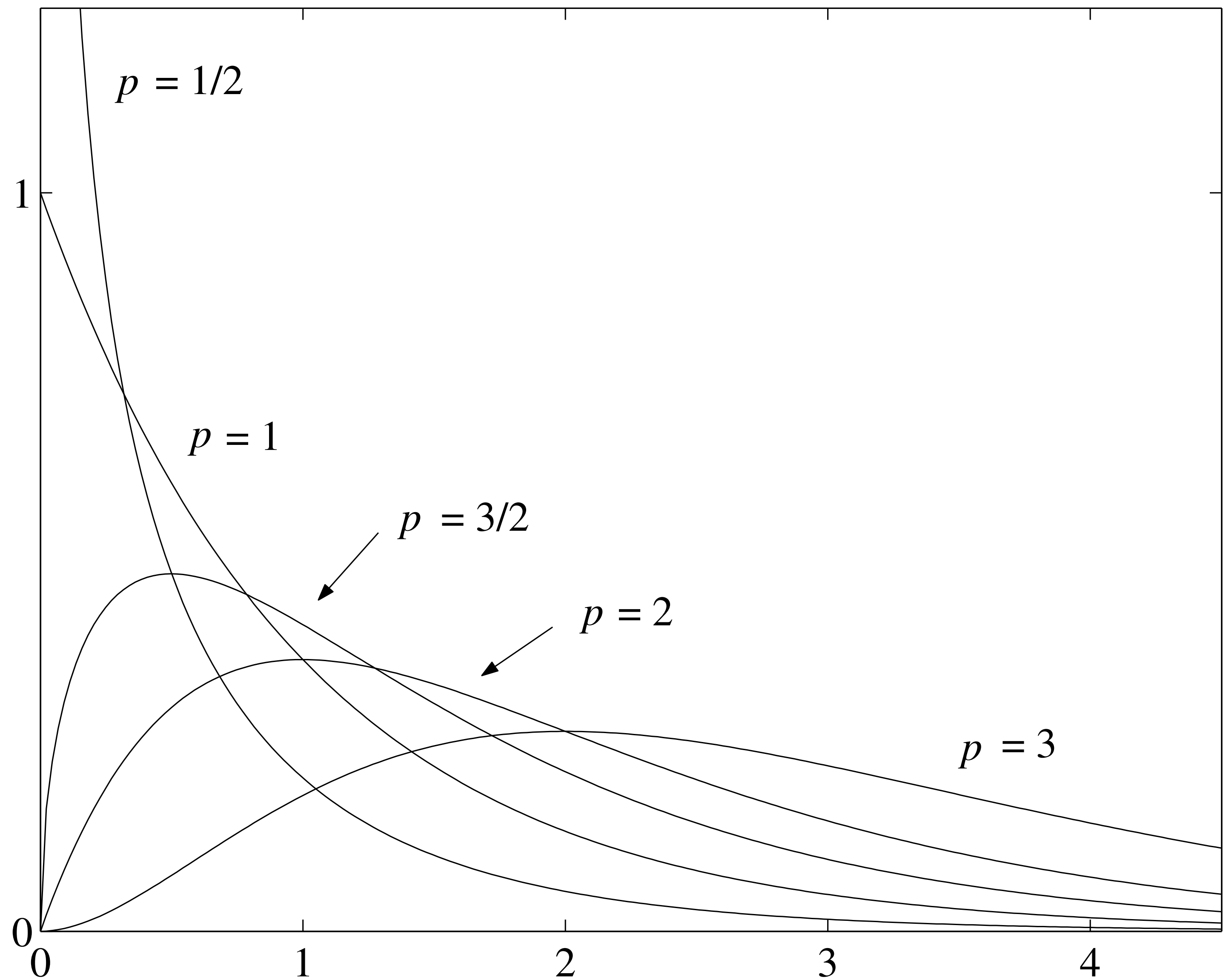

***Figure* 4.7.** The gamma densities $g_p(x)$ for $p = 1/2$, $p = 1$, $p = 3/2$, $p = 2$, and $p = 3$.

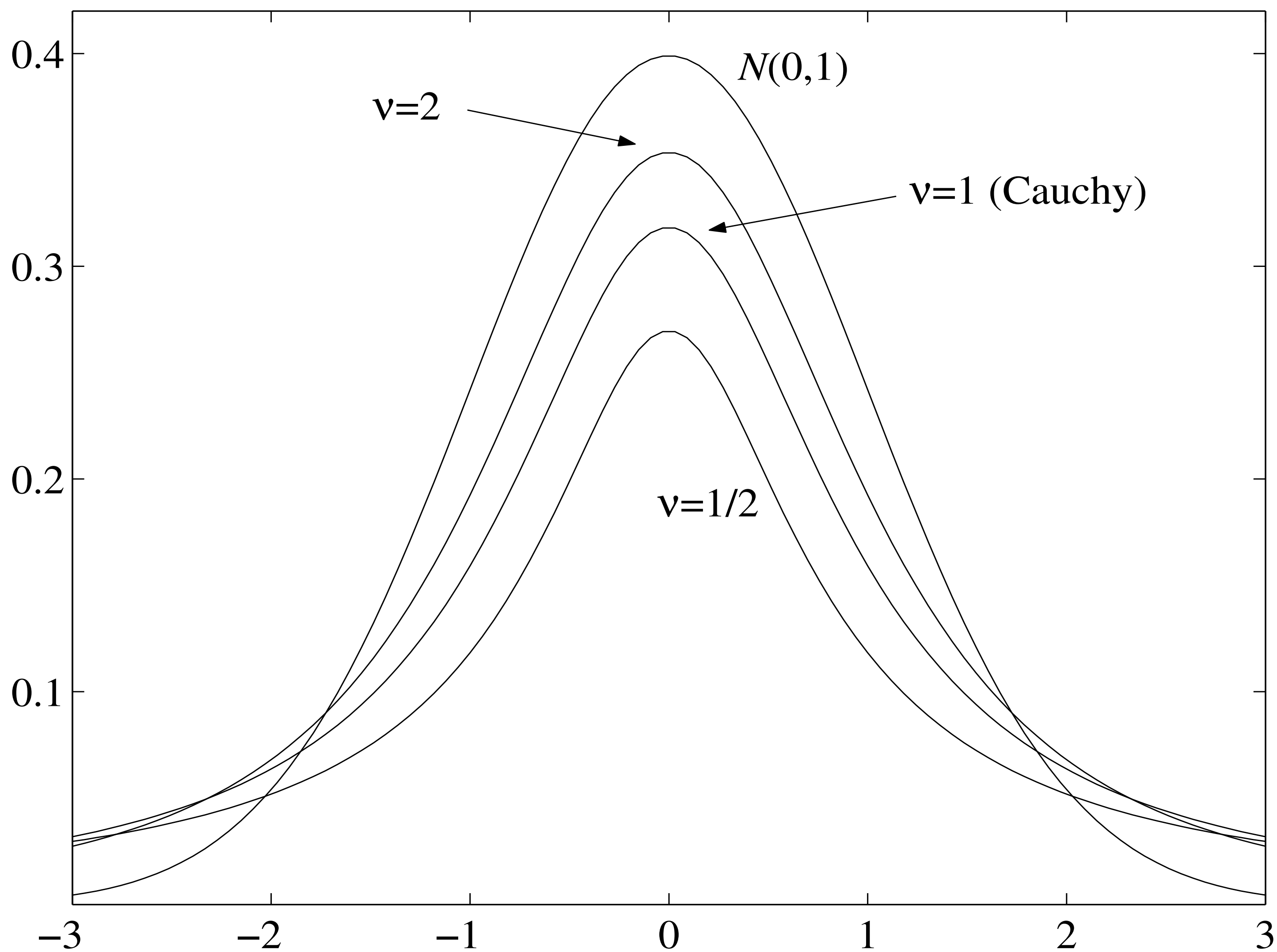

***Figure* 4.12.** Comparision of standard normal density and Student's t density for $\nu = 1/2$, 1, and 2.

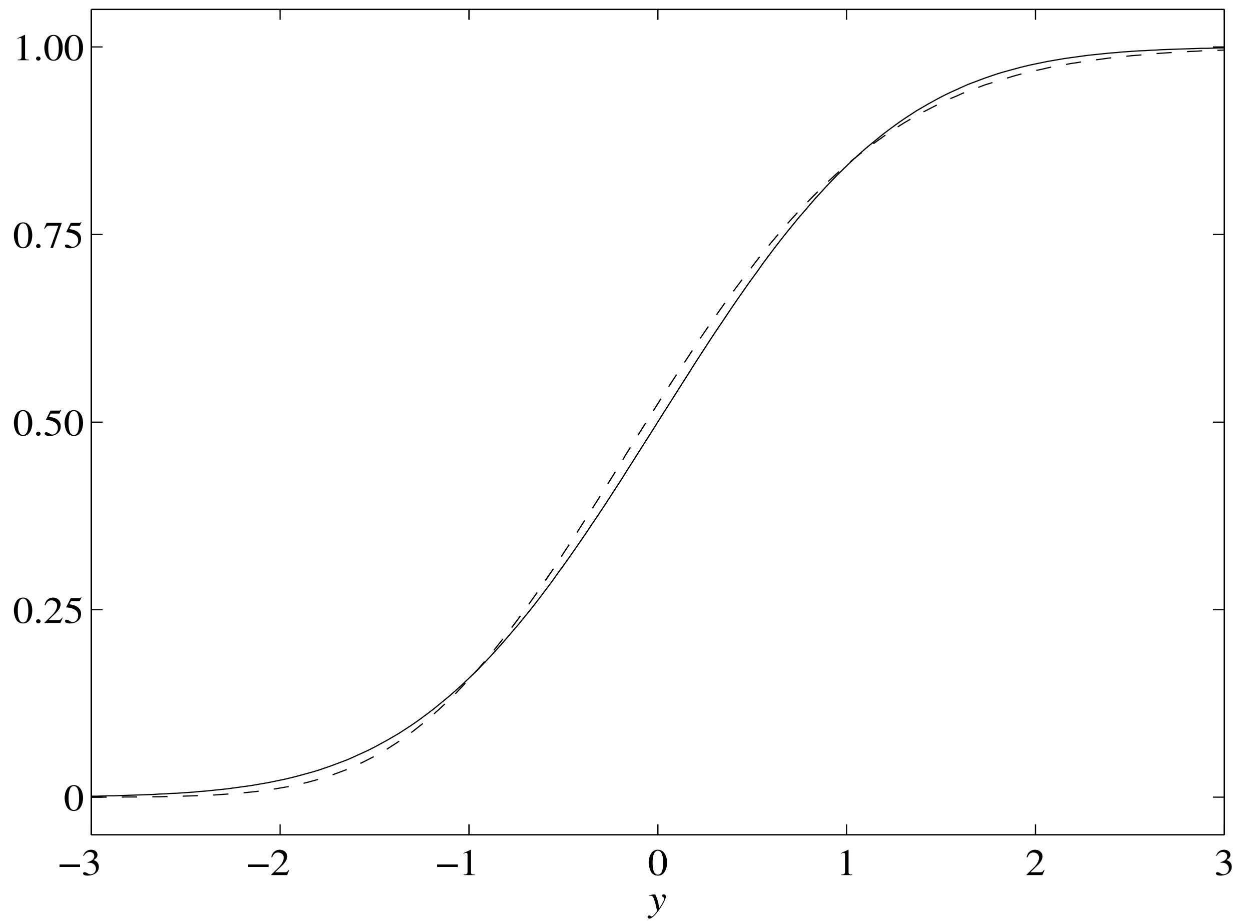

***Figure* 5.15.** Illustration of the central limit theorem when the X_i are exponential with parameter 1. The dashed line is $F_{Y_{30}}(y)$, and the solid line is the standard normal cumulative distribution, $\Phi(y)$.

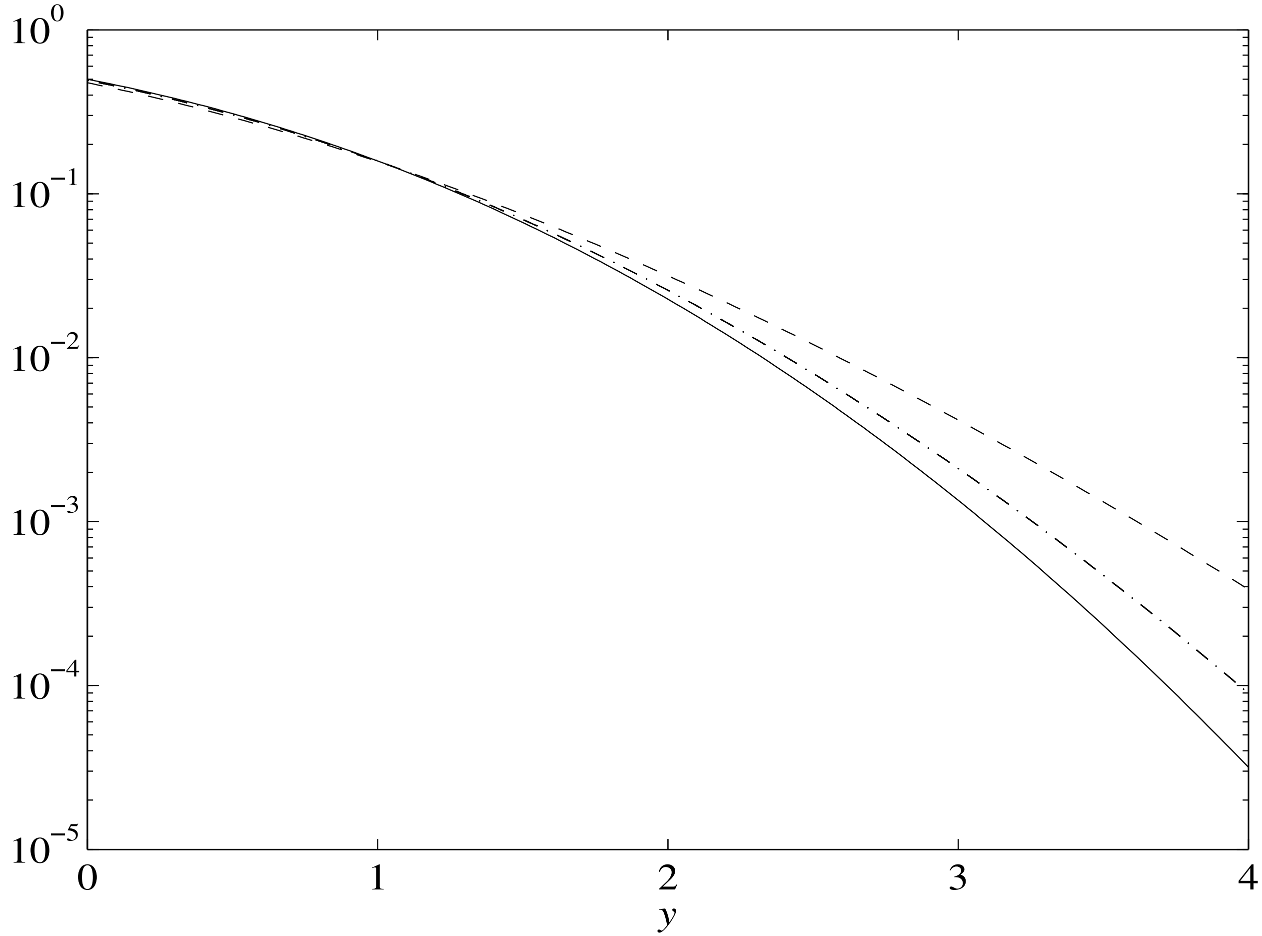

***Figure* 5.16.** Plots of $\log_{10}(1-F_{Y_{30}}(y))$ (dashed line), $\log_{10}(1-F_{Y_{300}}(y))$ (dash-dotted line), and $\log_{10}(1-\Phi(y))$ (solid line).

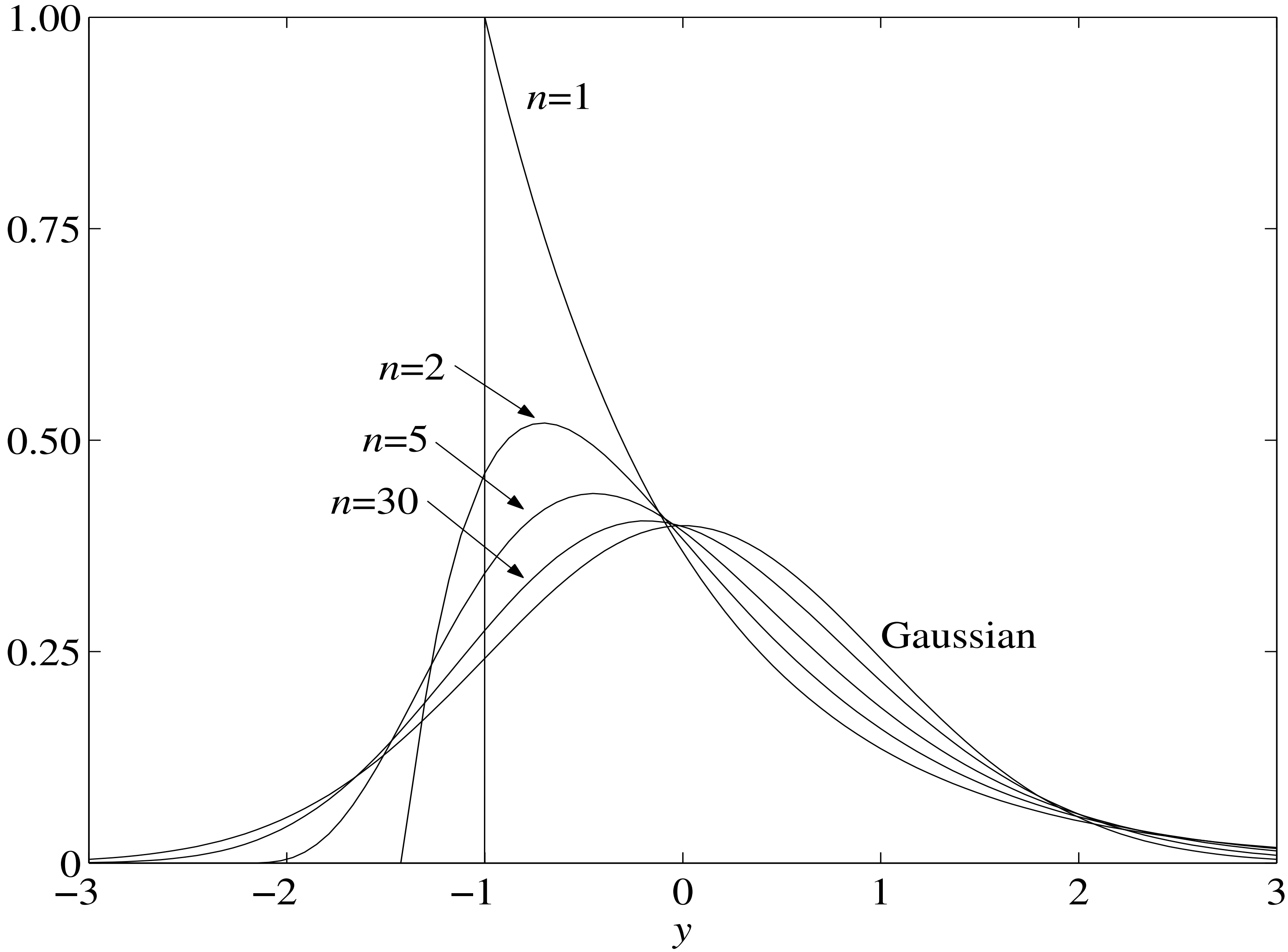

***Figure* 5.17.** For X_i i.i.d. $\exp(1)$, sketch of $f_{Y_n}(y)$ for $n = 1, 2, 5, 30$ and the $N(0, 1)$ density.

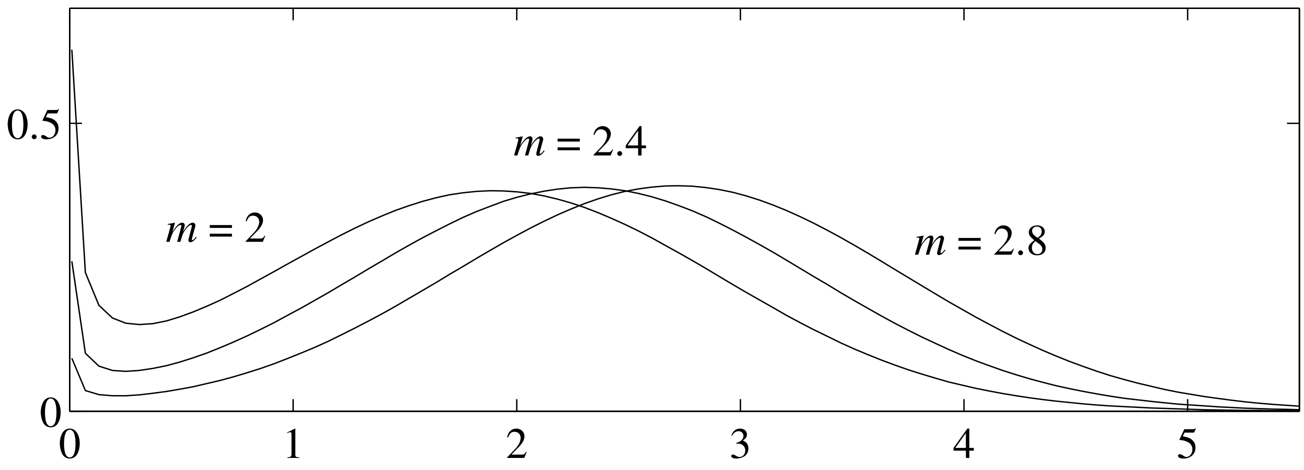

***Figure* 5.19.** Rice density $f_{Z_{1/2}}(z)$ for different values of m.

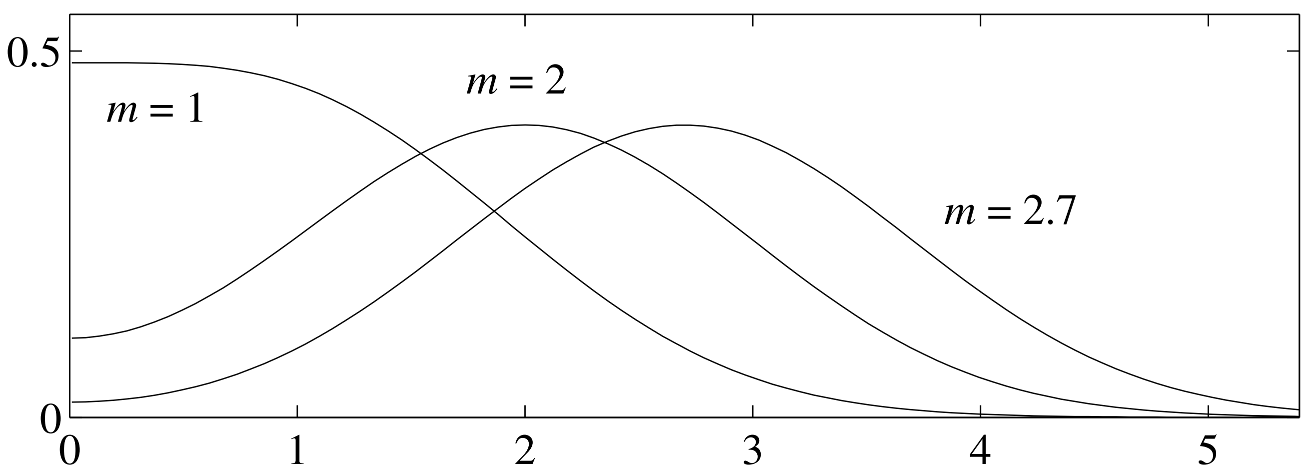

***Figure* 5.20.** Rice density $f_{Z_1}(z)$ for different values of m.

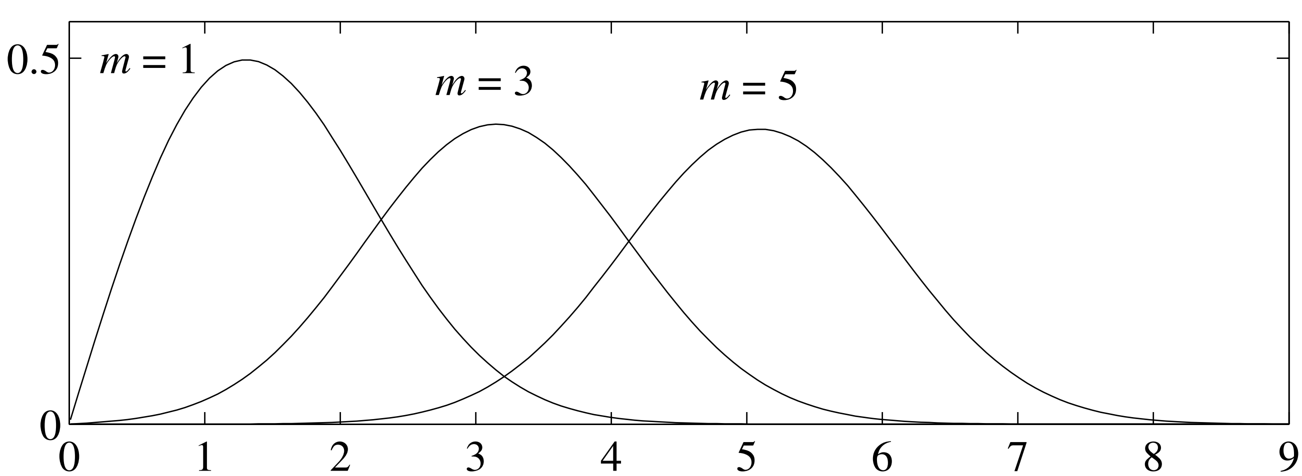

***Figure* 5.21.** Rice density $f_{Z_2}(z)$ for different values of m.

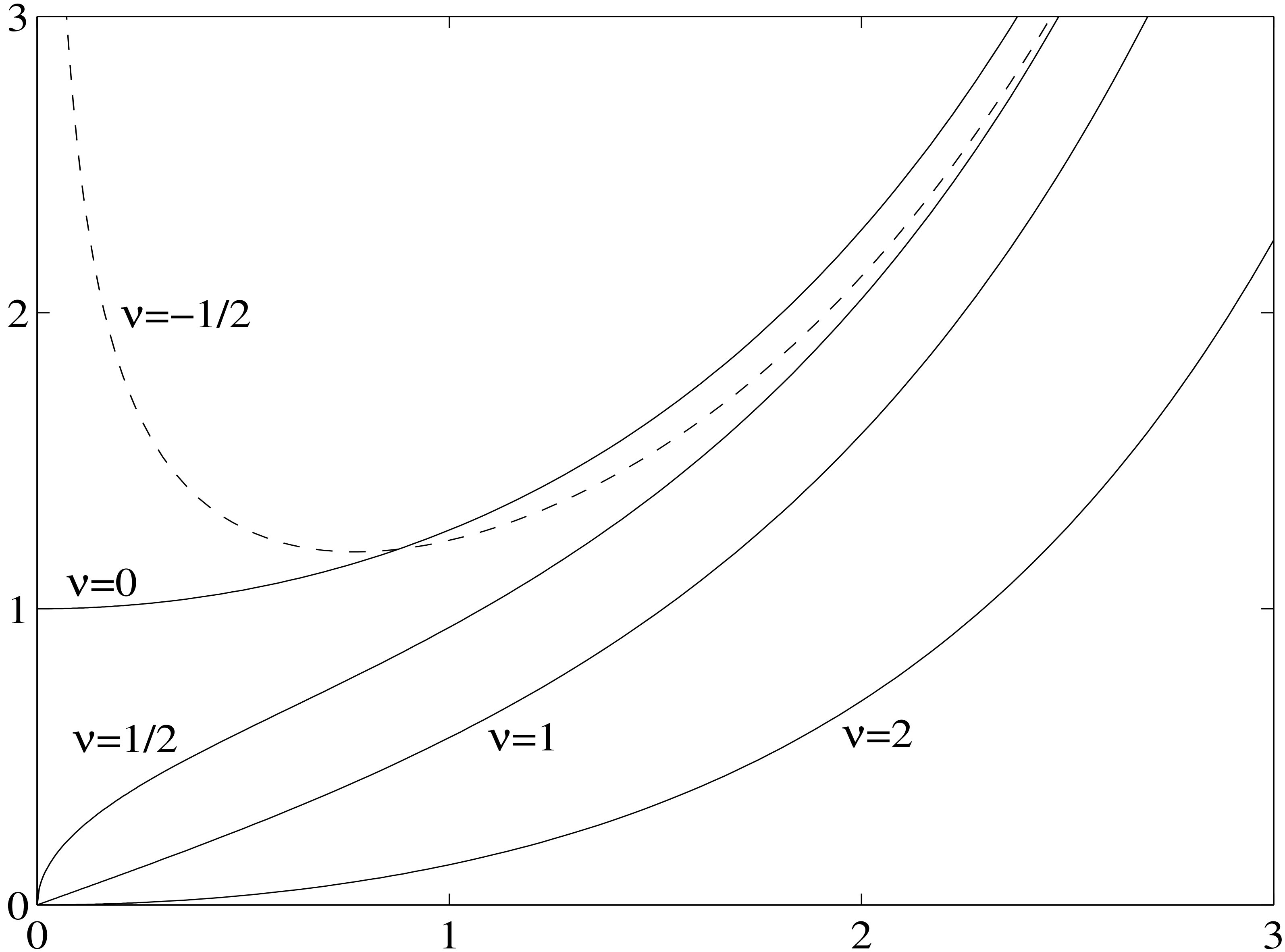

***Figure* 5.22.** Graphs if $I_\nu(x)$ for different values of ν.

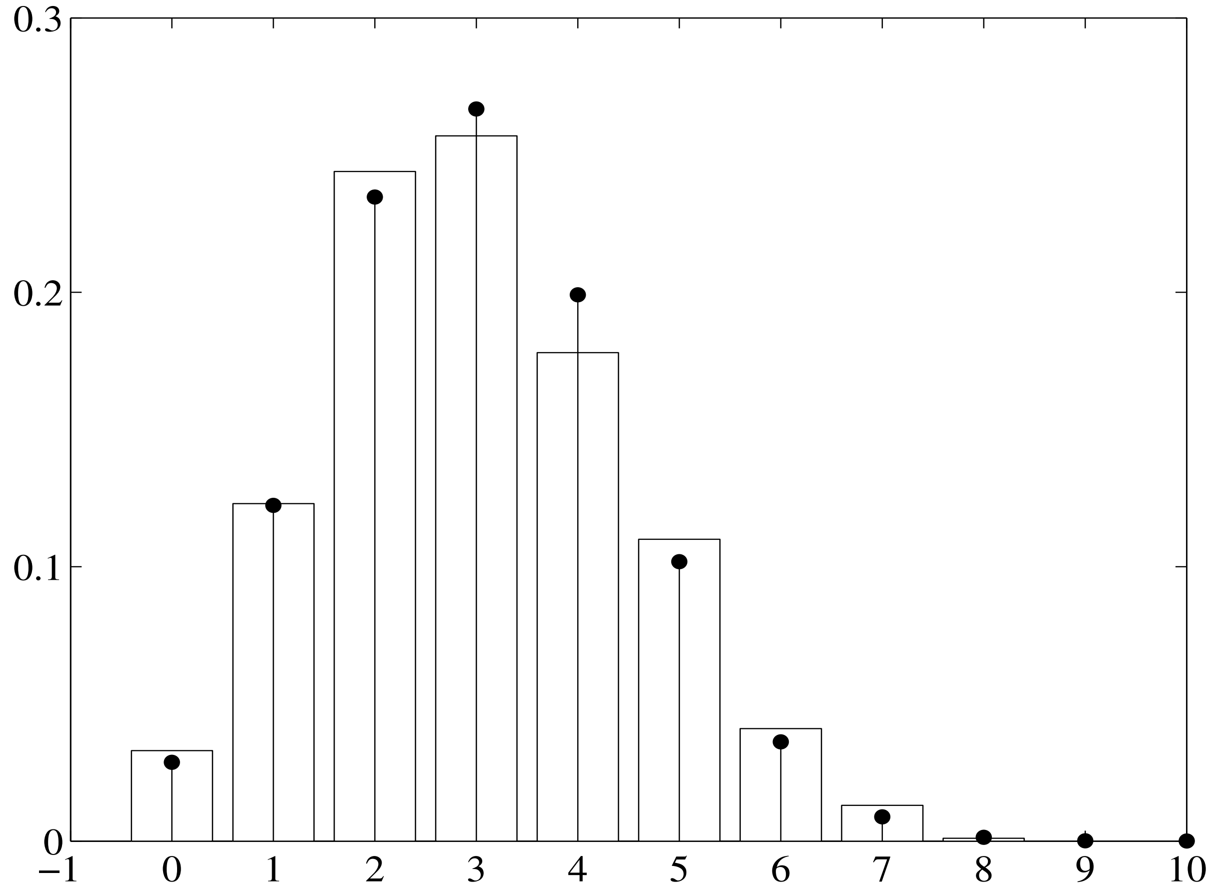

***Figure* 6.1.** Normalized histogram of 1000 i.i.d. binomial$(10, 0.3)$ random numbers. Stem plot shows pmf using $p_n = 0.2989$ estimated from the data.

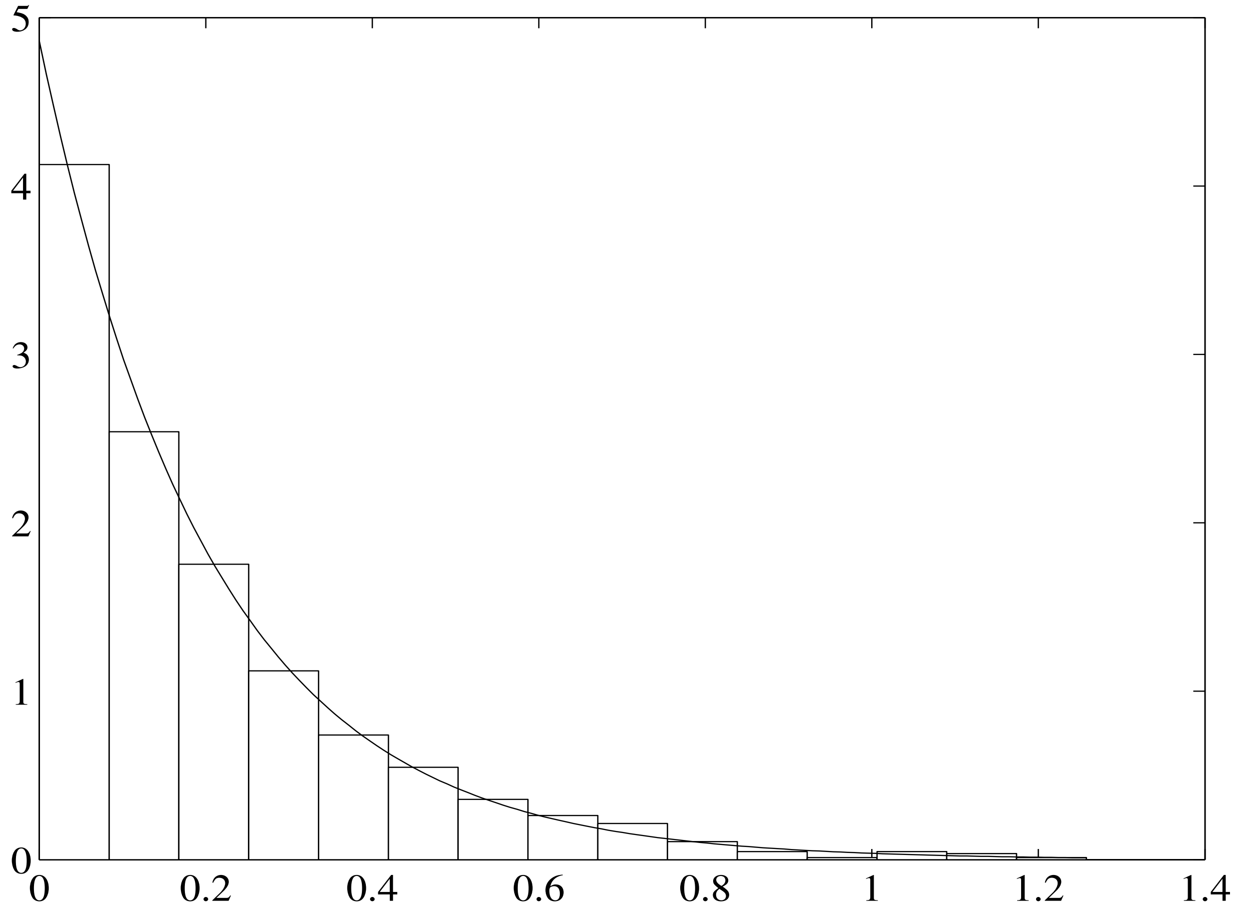

***Figure* 6.2.** Normalized histogram of 1000 i.i.d. exponential random numbers and the $\exp(\lambda)$ density with the value of λ estimated from the data.

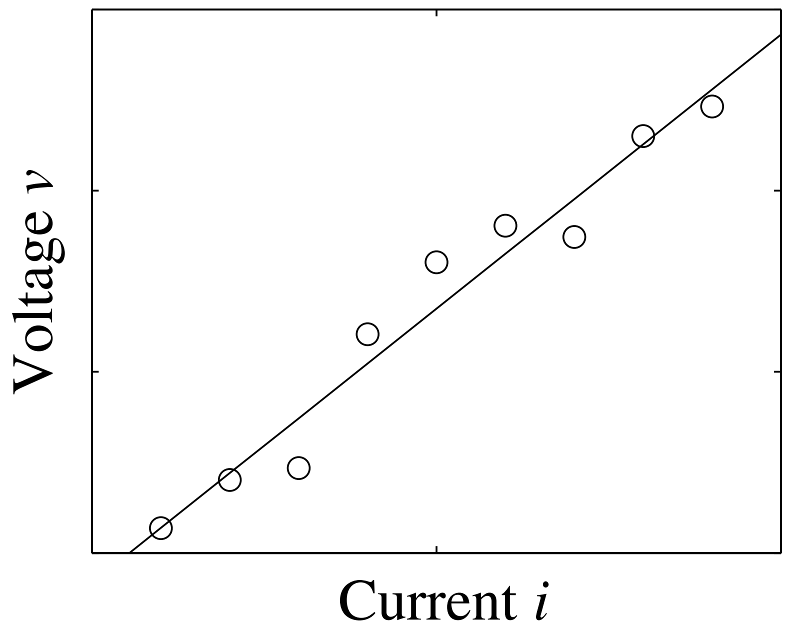

***Figure* 6.6.** Best-fit line through points in Figure 6.5.

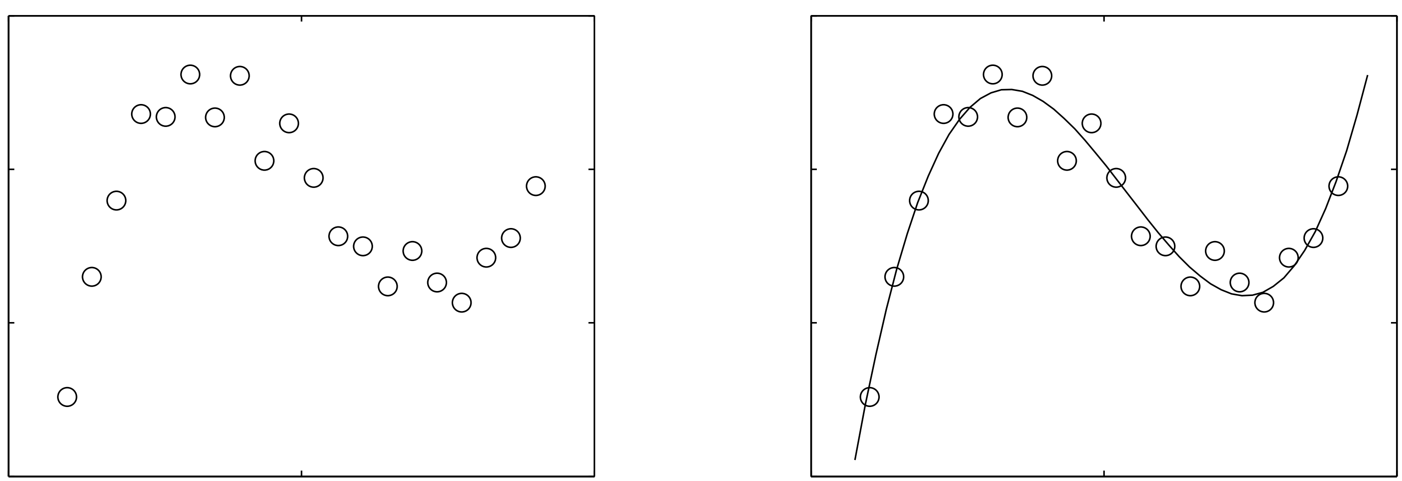

***Figure* 6.7.** Scatter plot (left) and best-fit cubic (right).

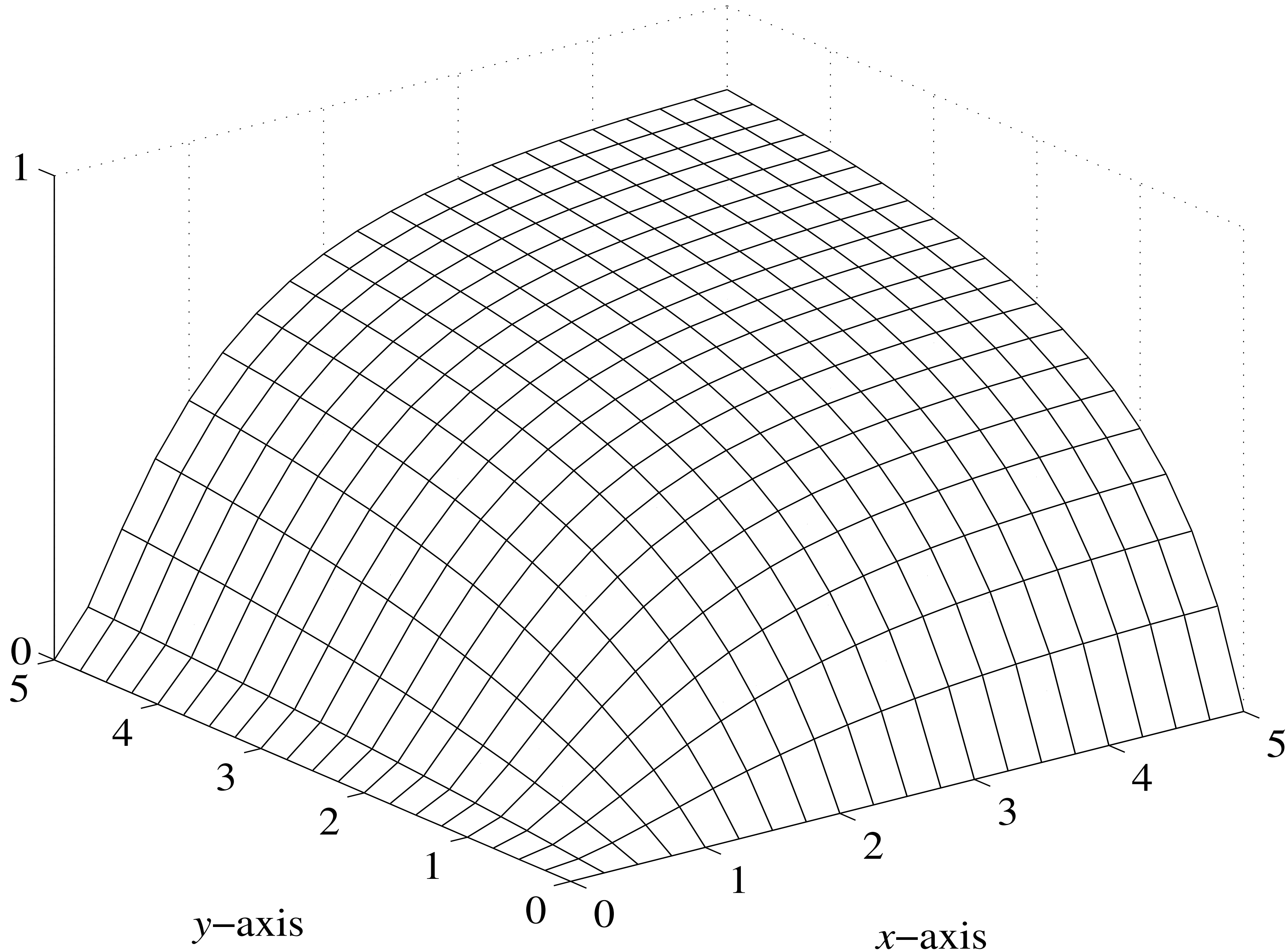

***Figure* 7.7.** Joint cumulative distribution function $F_{XY}(x, y)$ of Example 7.7.

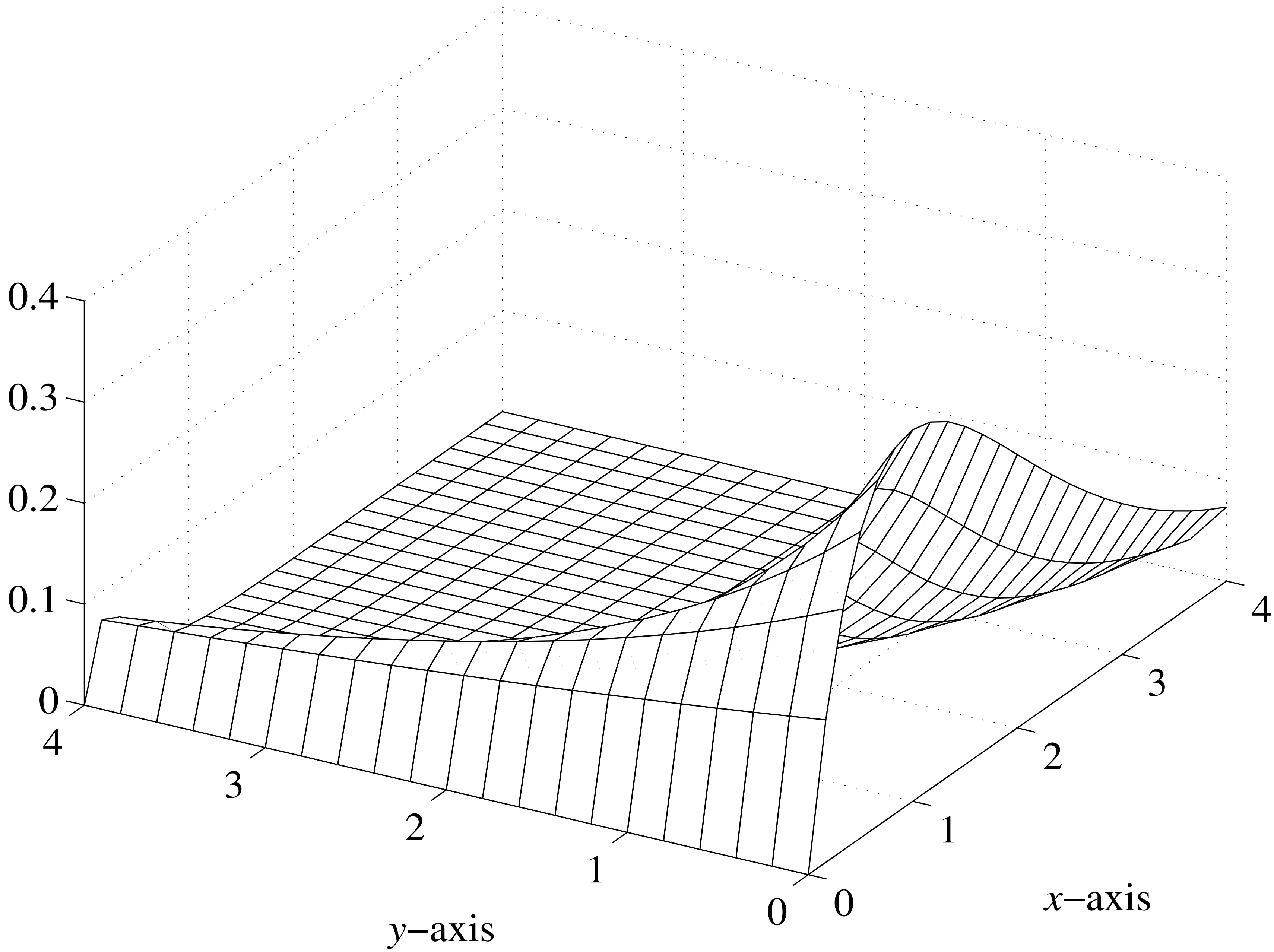

***Figure* 7.8.** The joint density $f_{XY}(x,y) = xe^{-x(y+1)}$ of Example 7.12.

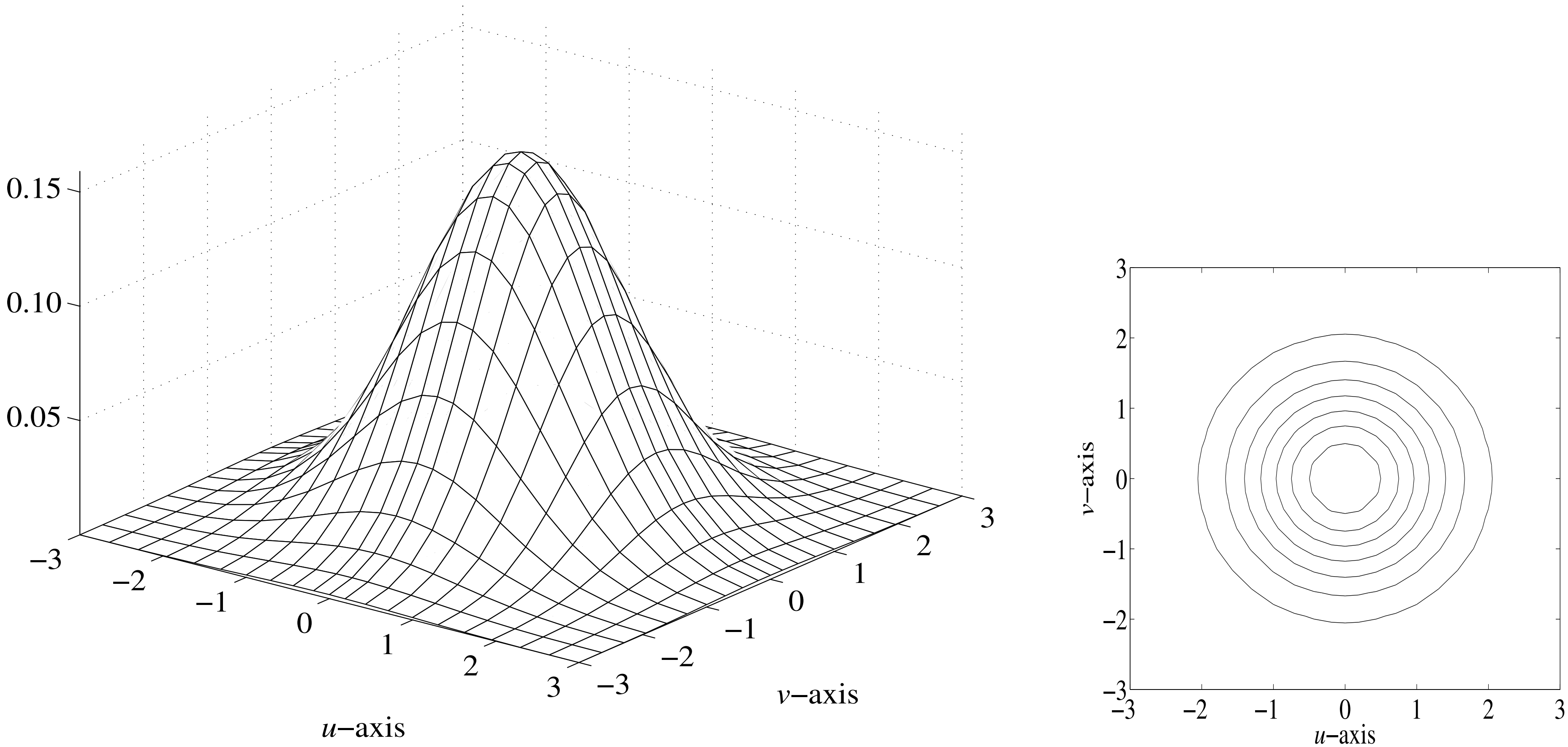

***Figure* 7.9.** The Gaussian surface $\psi_\rho(u,v)$ of (7.22) with $\rho = 0$ (left). The corresponding level curves (right).

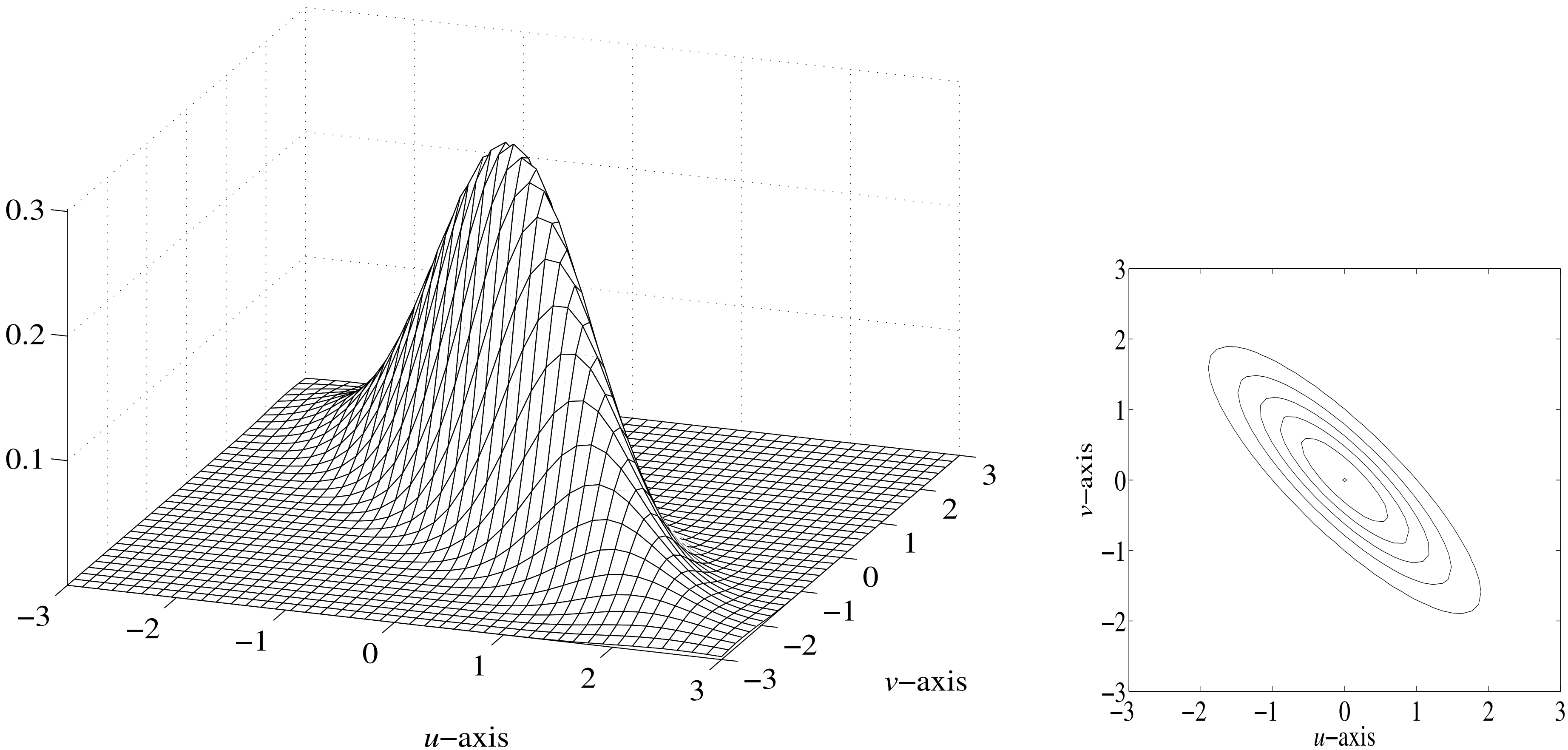

***Figure* 7.10.** The Gaussian surface $\psi_\rho(u,v)$ of (7.22) with $\rho = -0.85$ (left). The corresponding level curves (right).

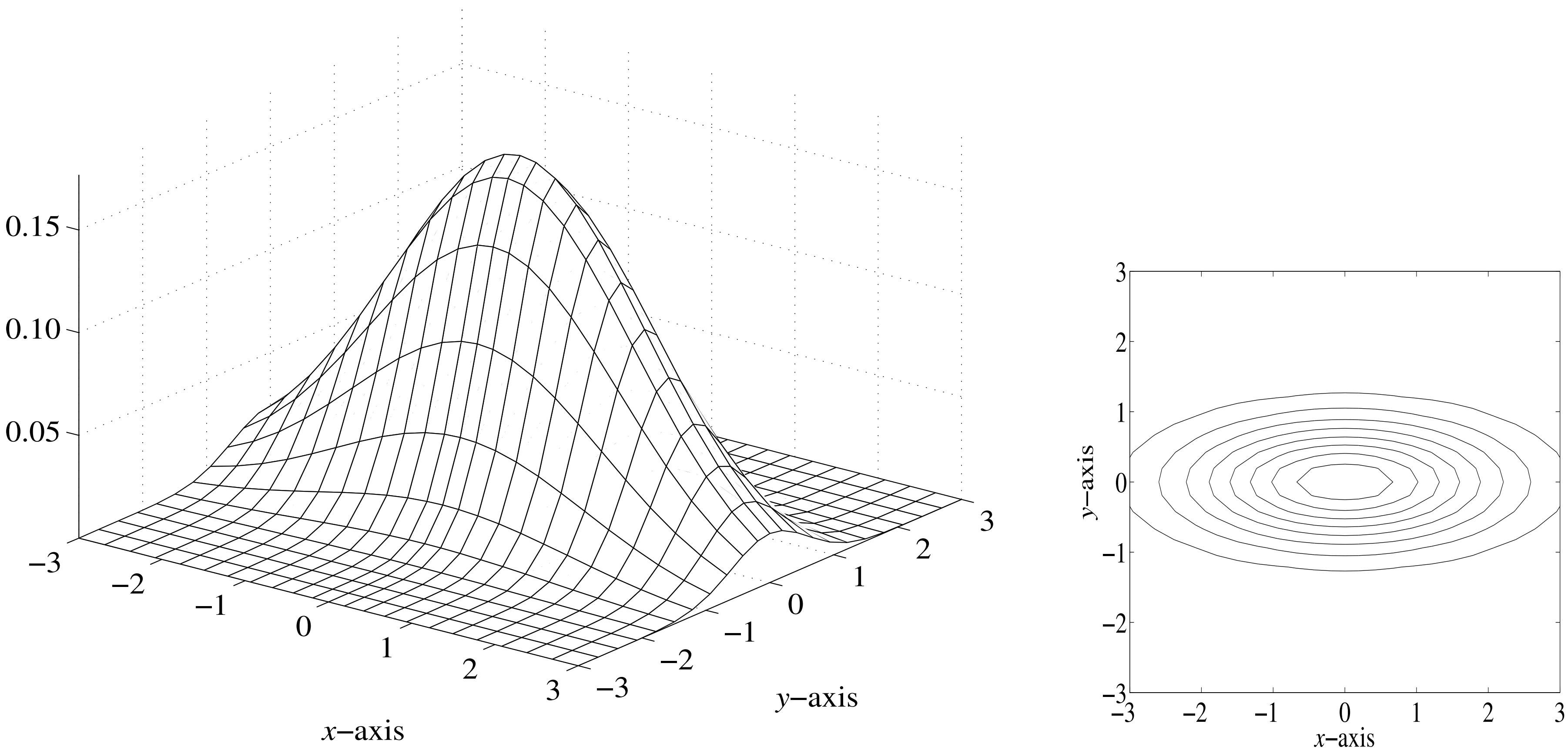

***Figure* 7.11.** The bivariate normal density $f_{XY}(x,y)$ of (7.25) with $m_X = m_Y = 0$, $\sigma_X = 1.5$, $\sigma_Y = 0.6$, and $\rho = 0$ (left). The corresponding level curves (right).

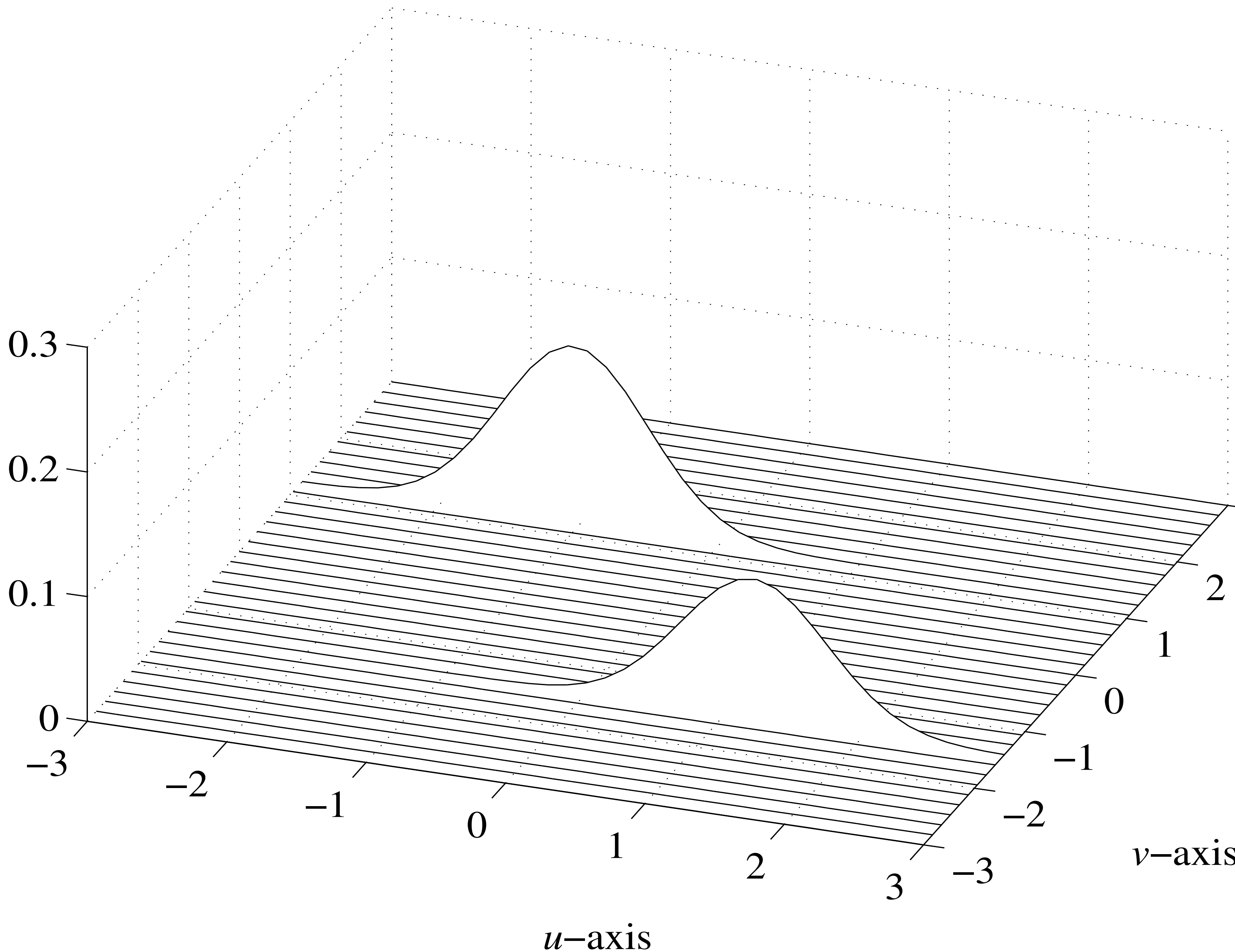

***Figure* 7.12.** Two slices from Figure 7.10.

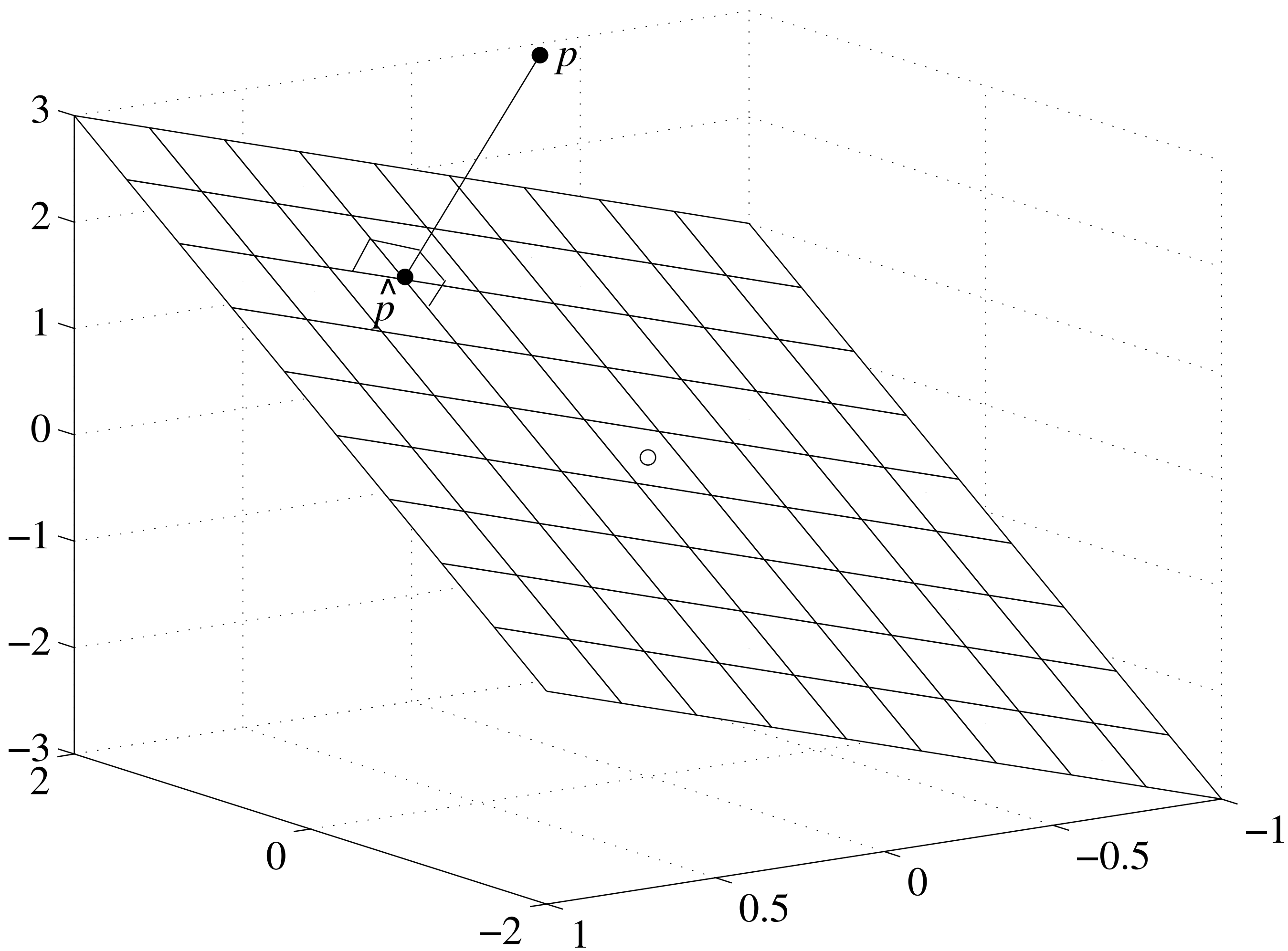

***Figure* 8.1.** The point on the plane that is closest to p is called the projection of p, and is denoted by $\widehat{p}$. The orthogonality principle says that $\widehat{p}$ is characterized by the property that the line joining $\widehat{p}$ to p is orthogonal to the plane. The symbol $\circ$ denotes the origin.

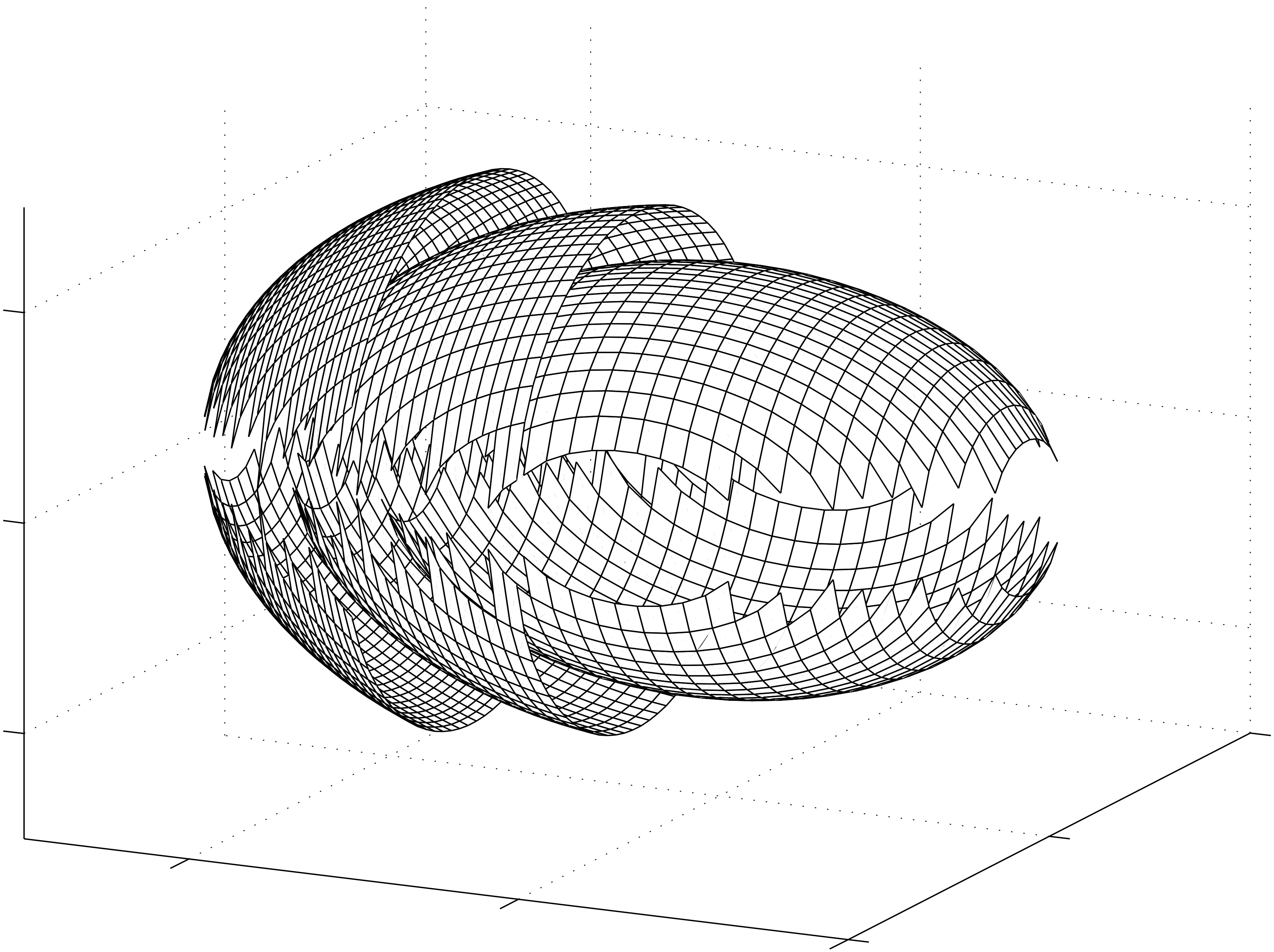

Figure **9.1.** Ellipsoid level surfaces of a three-dimensional Gaussian density.

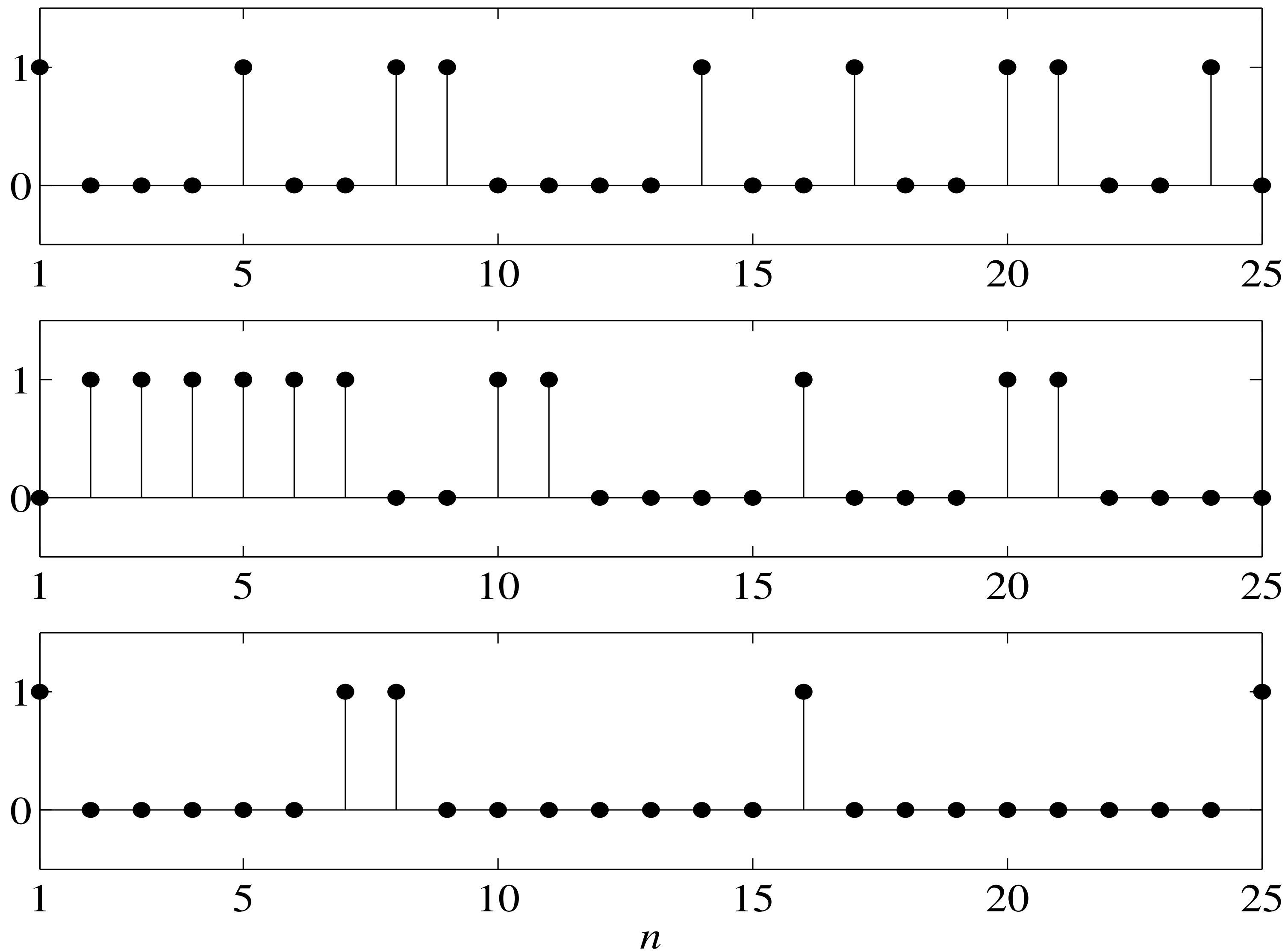

***Figure* 10.1.** Three realizations of an i.i.d. sequence of Bernoulli(p) random variables $\{X_n, n = 1, 2, \ldots\}$.

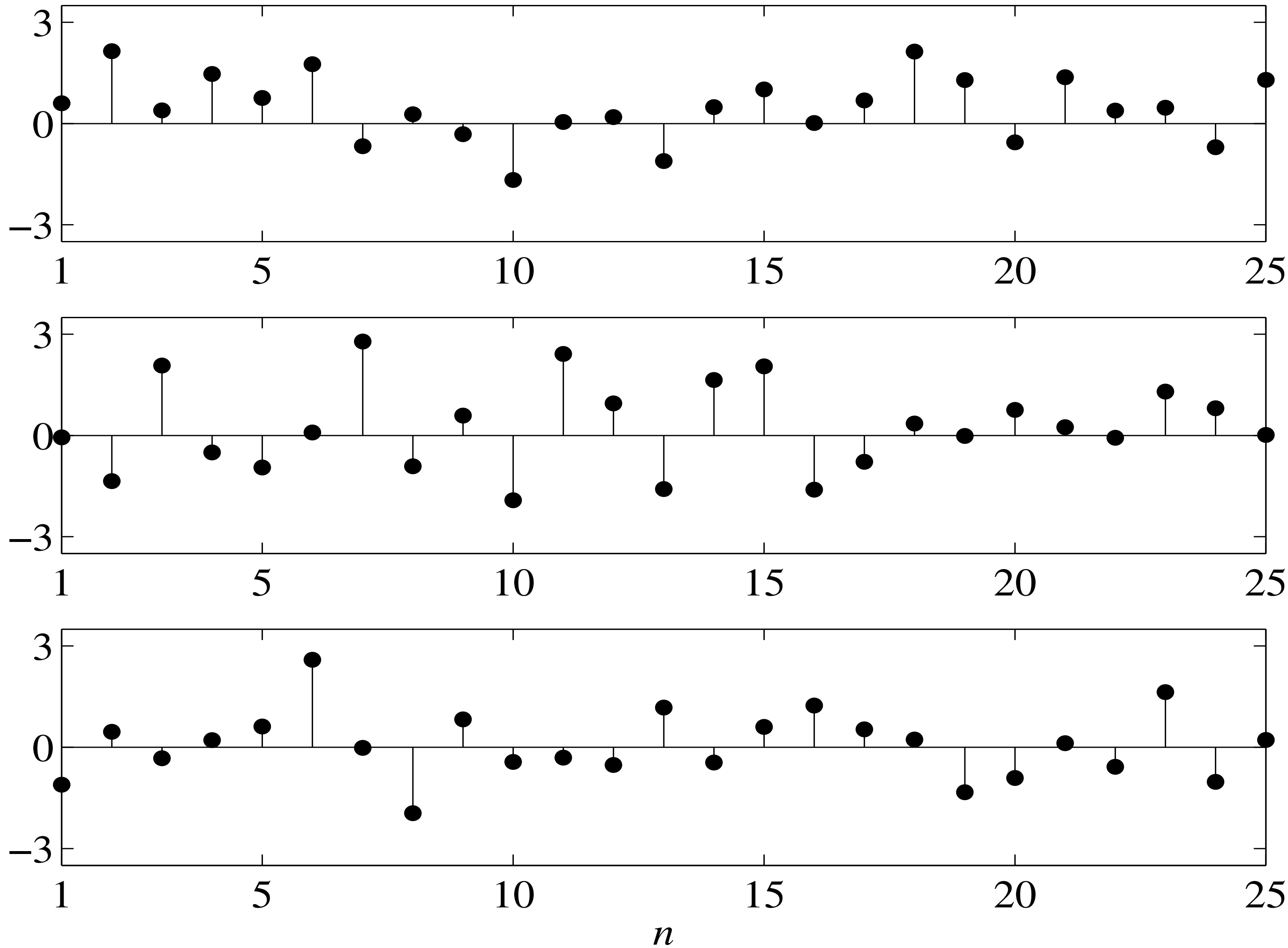

***Figure* 10.2.** Three realizations of an i.i.d. sequence of $N(0,1)$ random variables $\{Z_n, n = 1, 2, \ldots\}$.

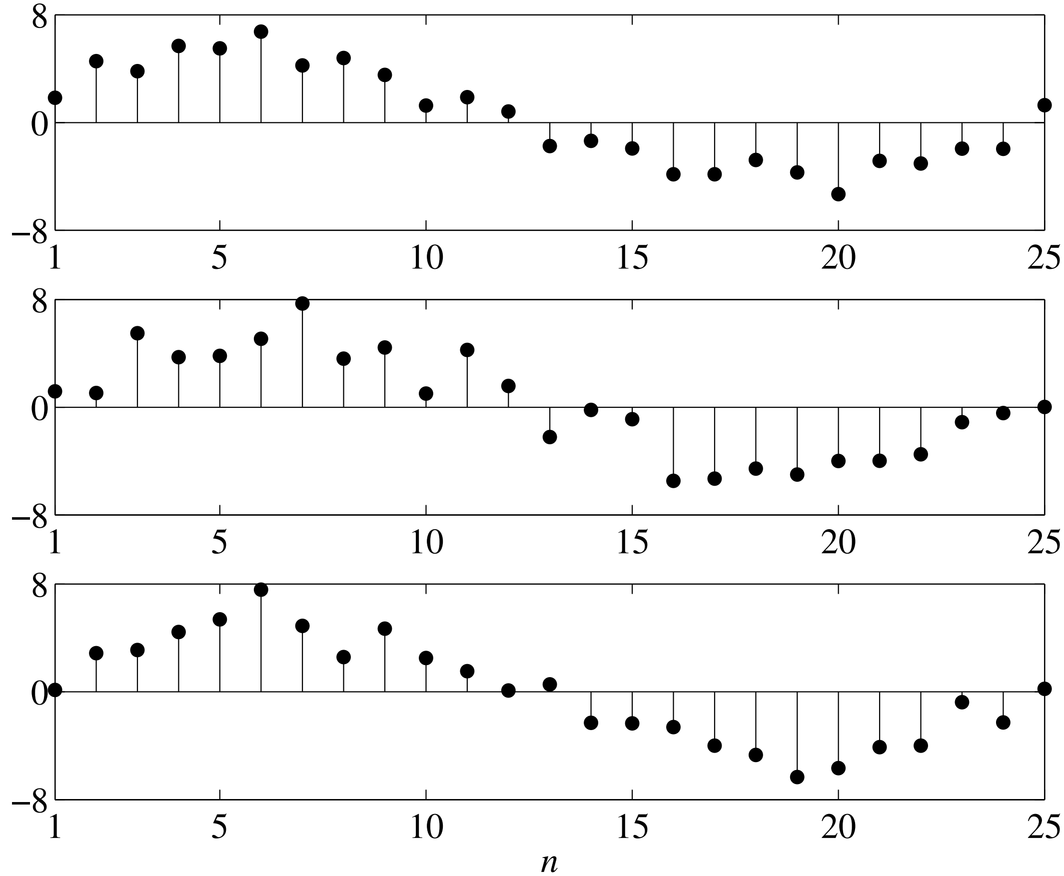

***Figure* 10.3.** Three realizations of $5\sin(2\pi fn) + Z_n$, where $f = 1/25$. The realizations of Z_n in this figure are the same as those in Figure 10.2.

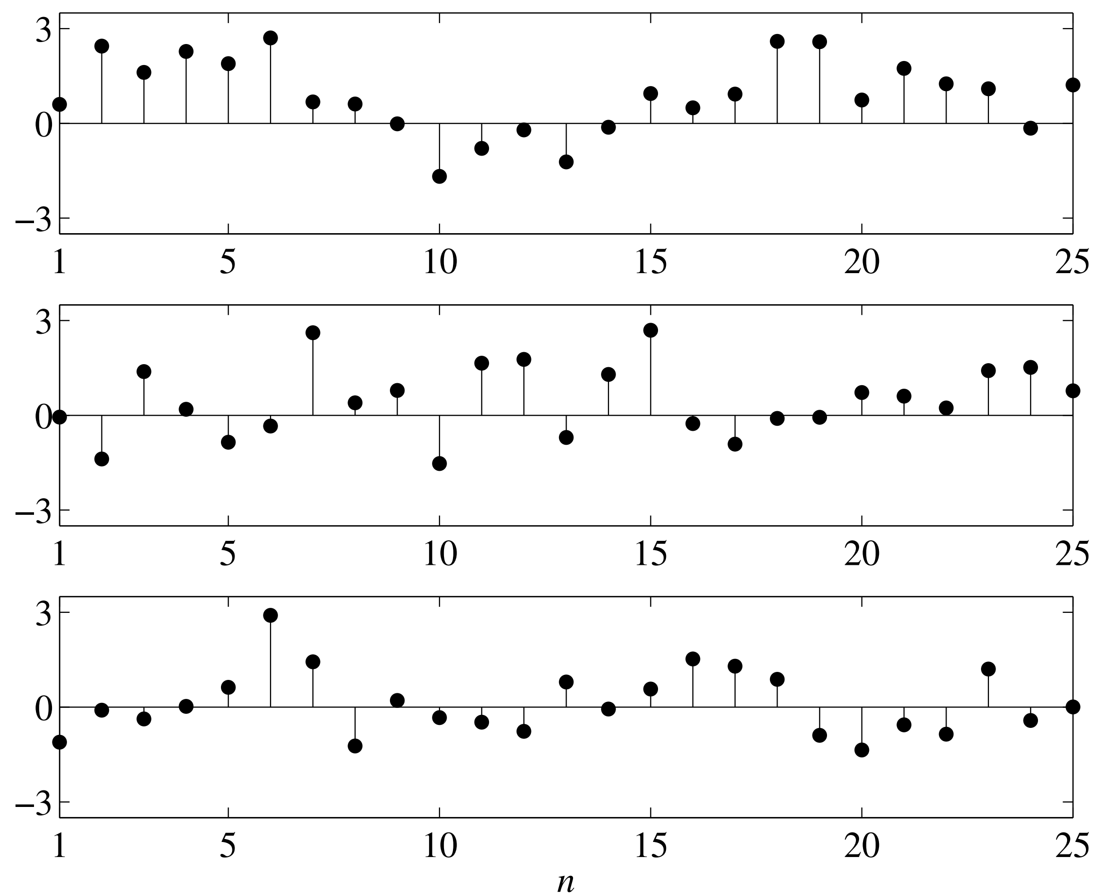

***Figure* 10.4.** Three realizations of $Y_n = \frac{1}{2}Y_{n-1} + Z_n$, where $Y_0 \equiv 0$. The realizations of Z_n in this figure are the same as those in Figure 10.2.

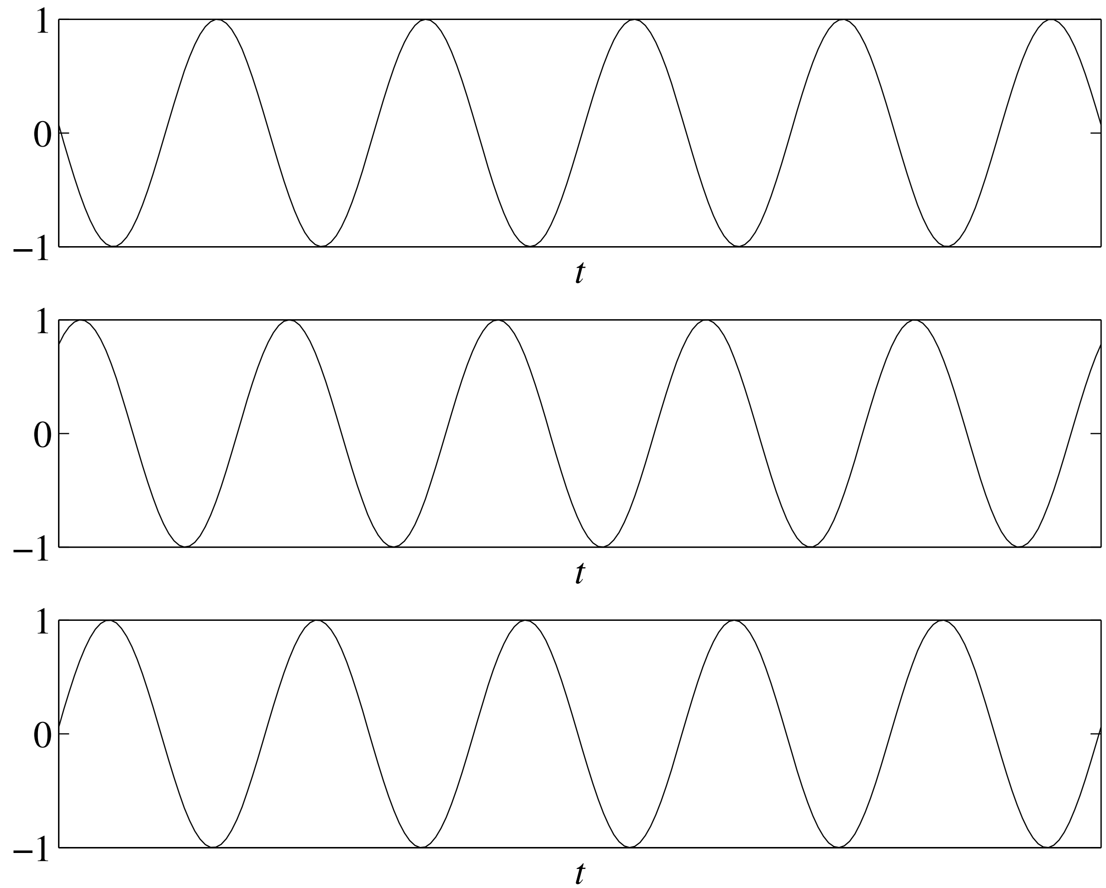

***Figure* 10.5.** Three realizations of the carrier with random phase, $X_t := \cos(2\pi f t + \Theta)$. The three different values of Θ are 1.5, -0.67, and -1.51, top to bottom, respectively.

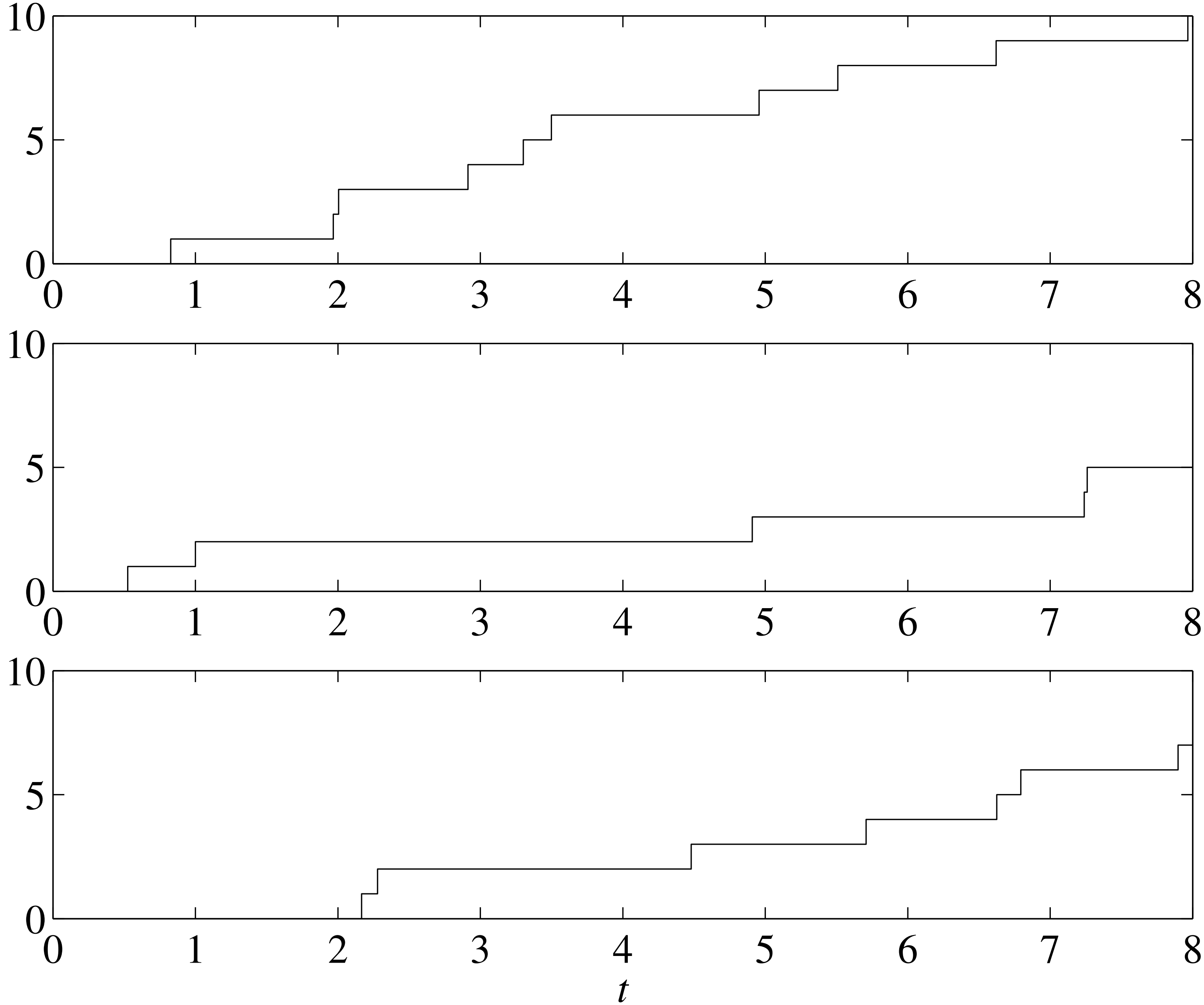

***Figure* 10.6.** Three realizations of a counting process N_t.

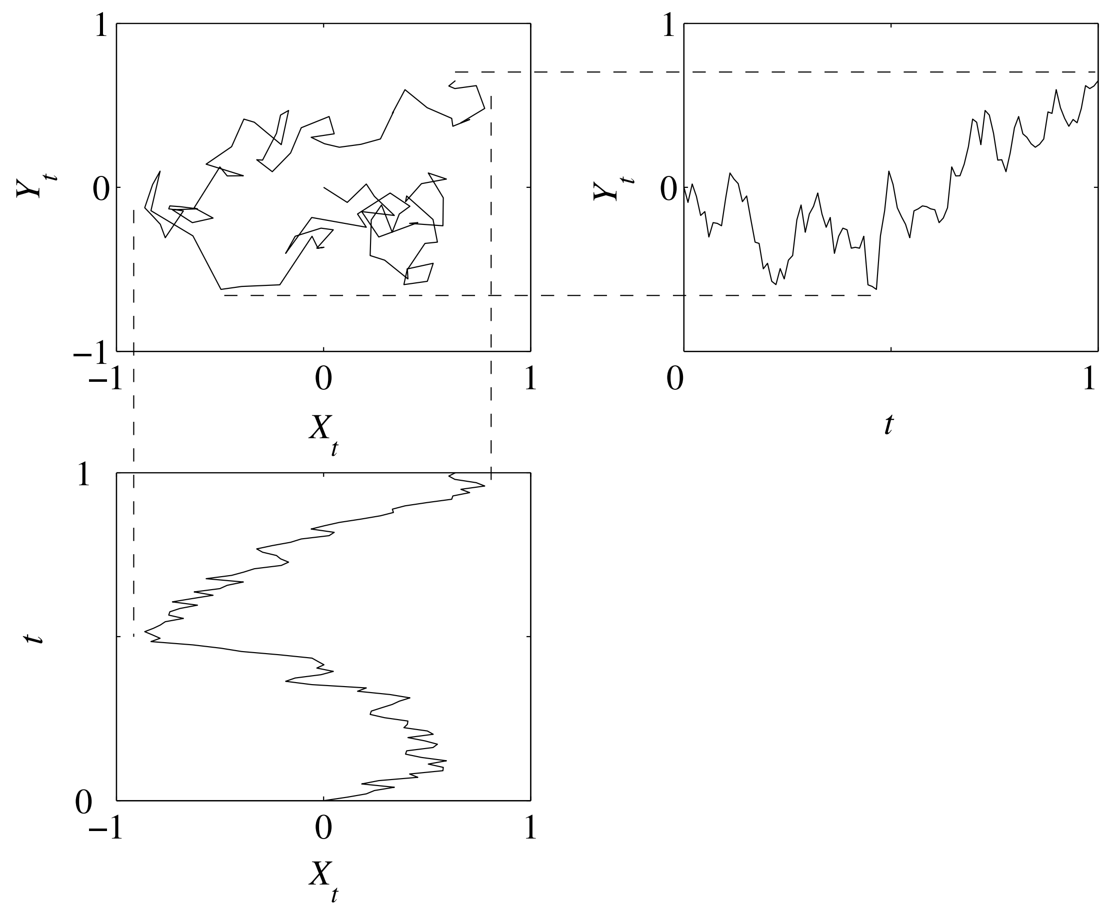

***Figure* 10.7.** The two-dimensional Brownian motion (X_t, Y_t) is shown in the upper-left plot; the curve starts in the center of the plot at time $t = 0$ and ends at the upper right of the plot at time $t = 1$. The vertical component Y_t as a function of time is shown in the upper-right plot. The horizontal component X_t as a function of time is shown in the lower-left plot; *note here that the vertical axis is time and the horizontal axis is X_t.*

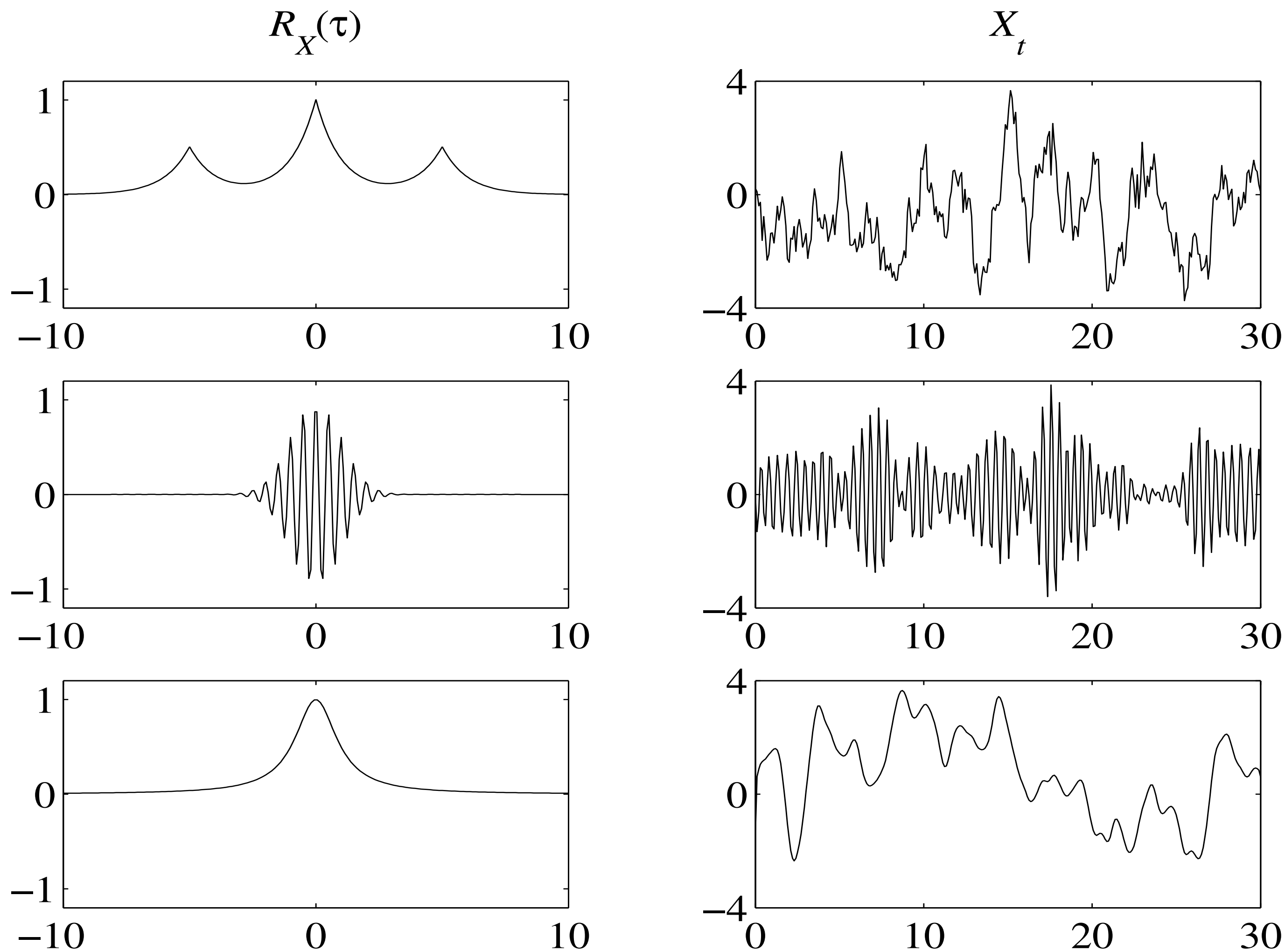

***Figure* 10.8.** Three examples of a correlation function with a sample path of a process with that correlation function.

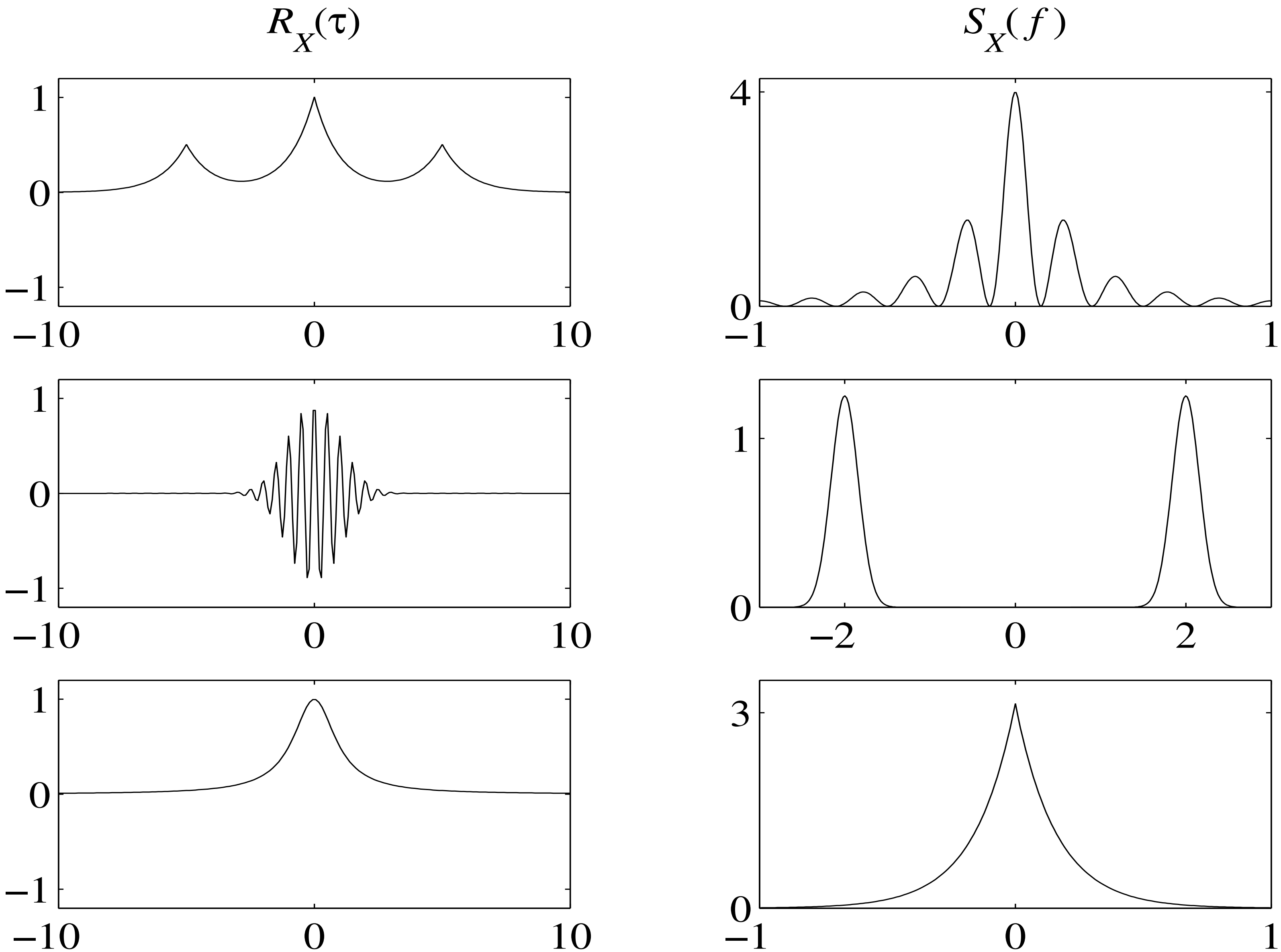

***Figure* 10.9.** Three correlation functions (left) and their corresponding Fourier transforms (right).

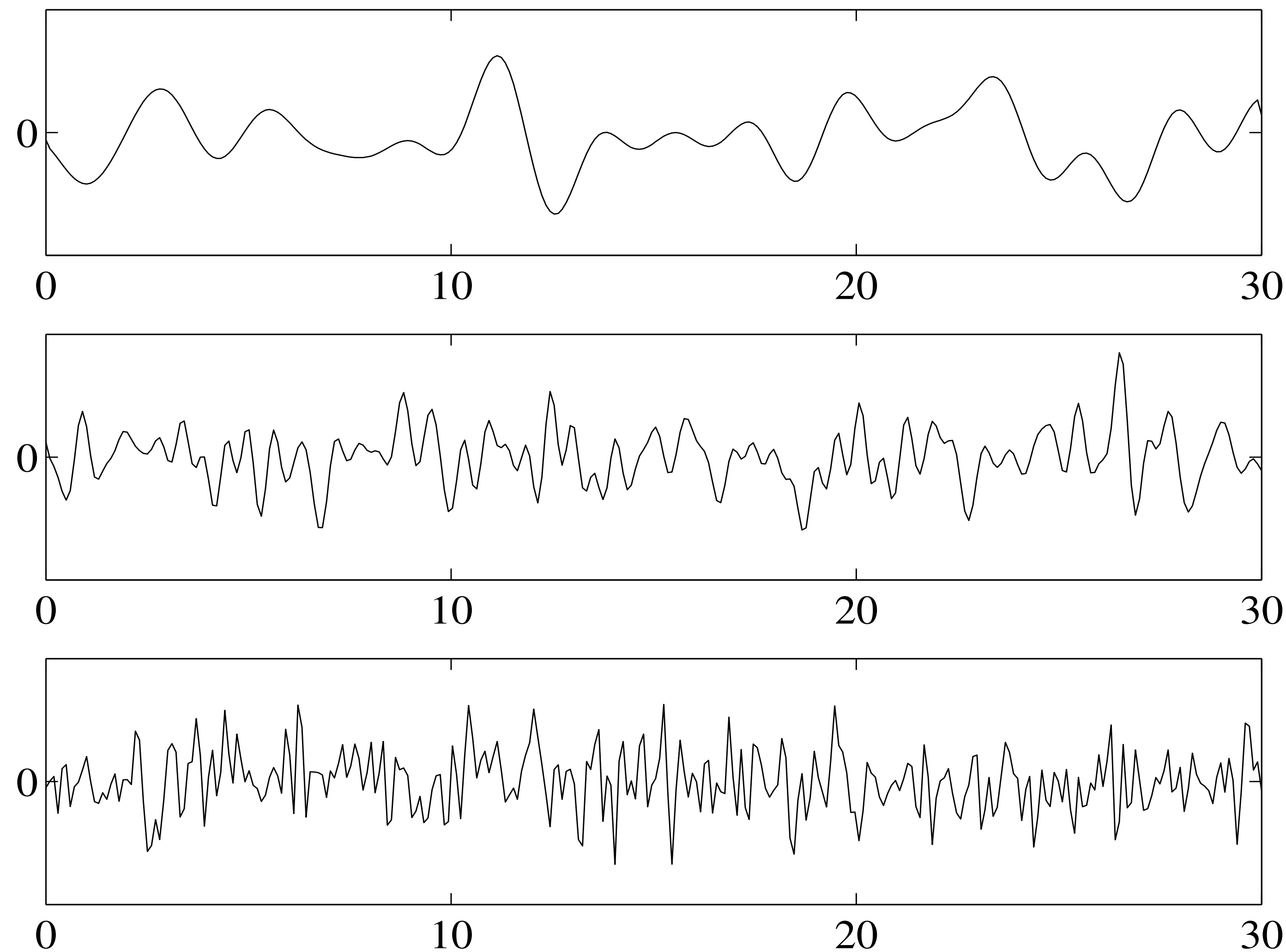

***Figure* 10.14.** Bandlimited white noise processes with the power spectral density in Figure 10.10 and the correlation function in Figure 10.11 for $W = 1/2$ (top), $W = 2$ (middle), and $W = 4$ (bottom).

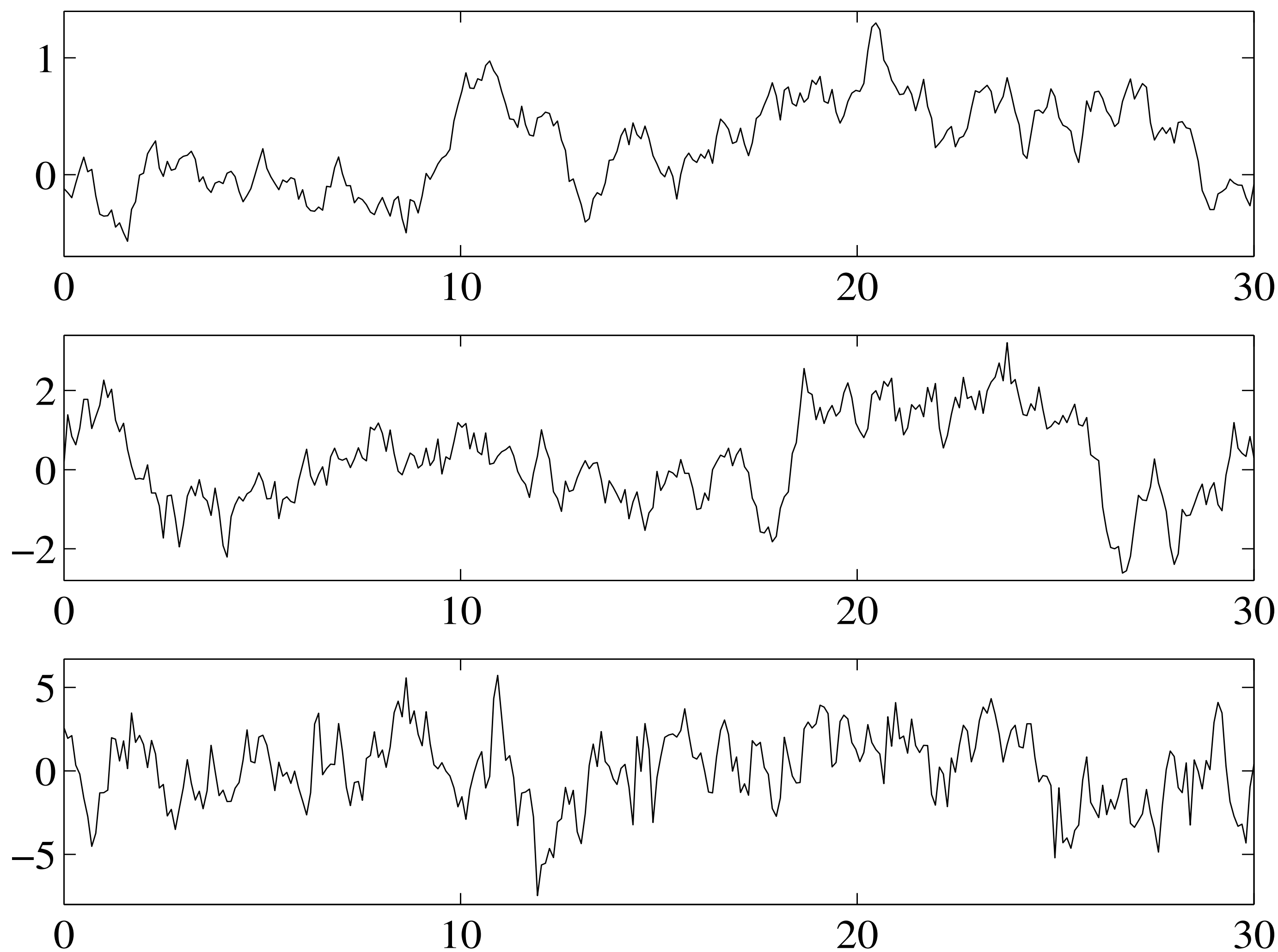

***Figure* 10.16.** Three realizations of a lowpass *RC* filter output driven by white noise. The time constants are $RC = 4$ (top), $RC = 1$ (middle), and $RC = 1/4$ (bottom).

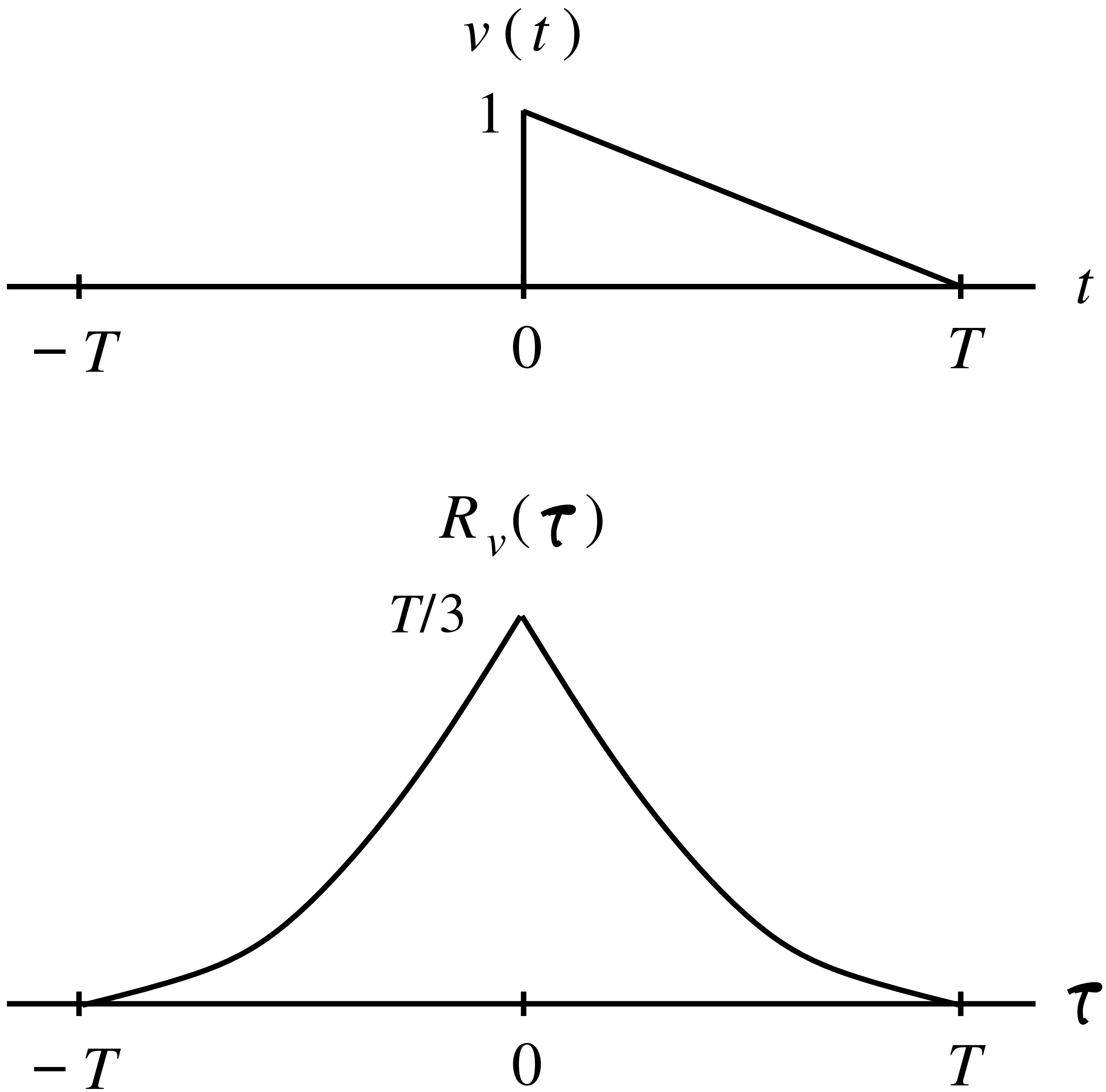

***Figure* 10.19.** Deterministic signal $v(t)$ and its correlation function $R_v(\tau)$.

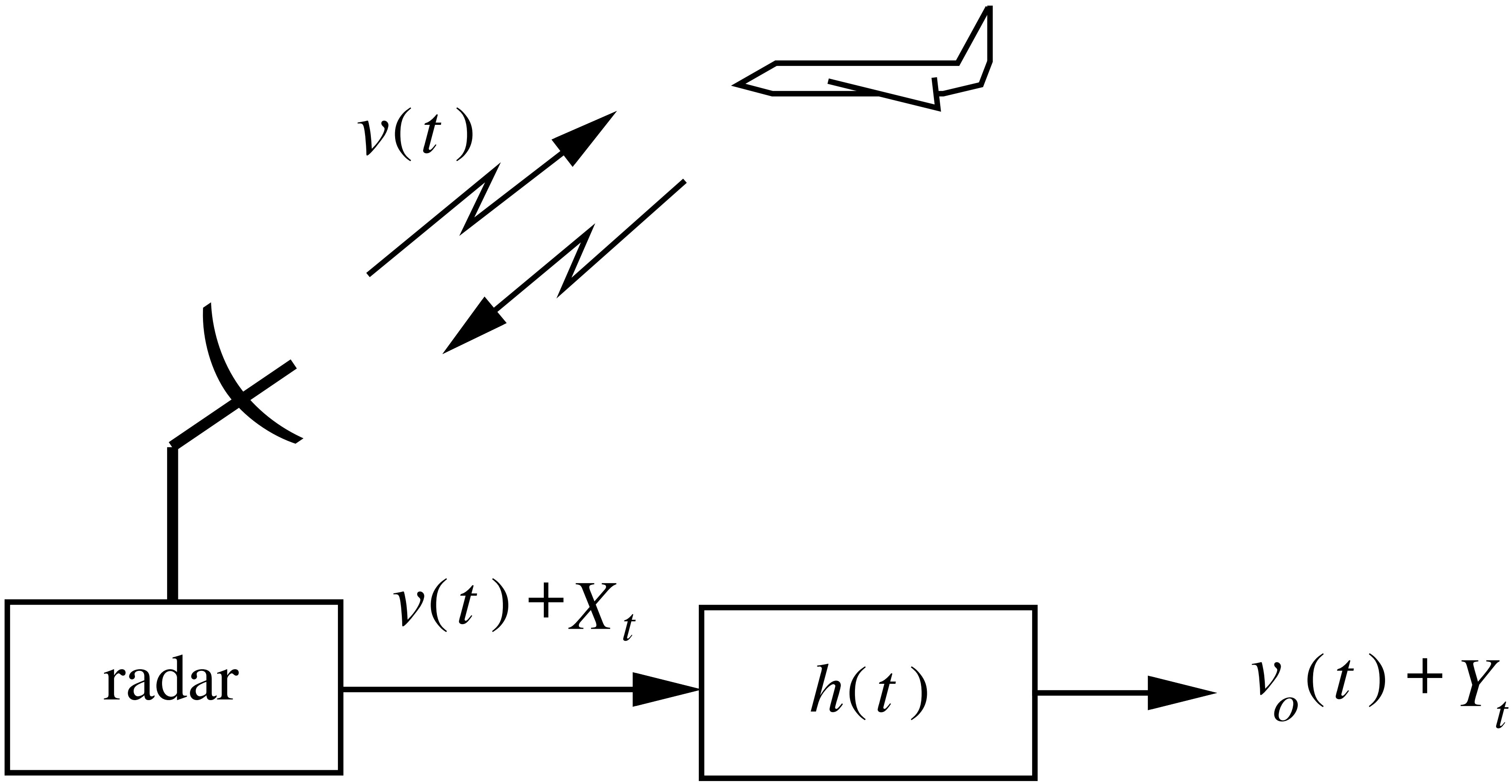

***Figure* 10.20.** Block diagram of radar system and matched filter.

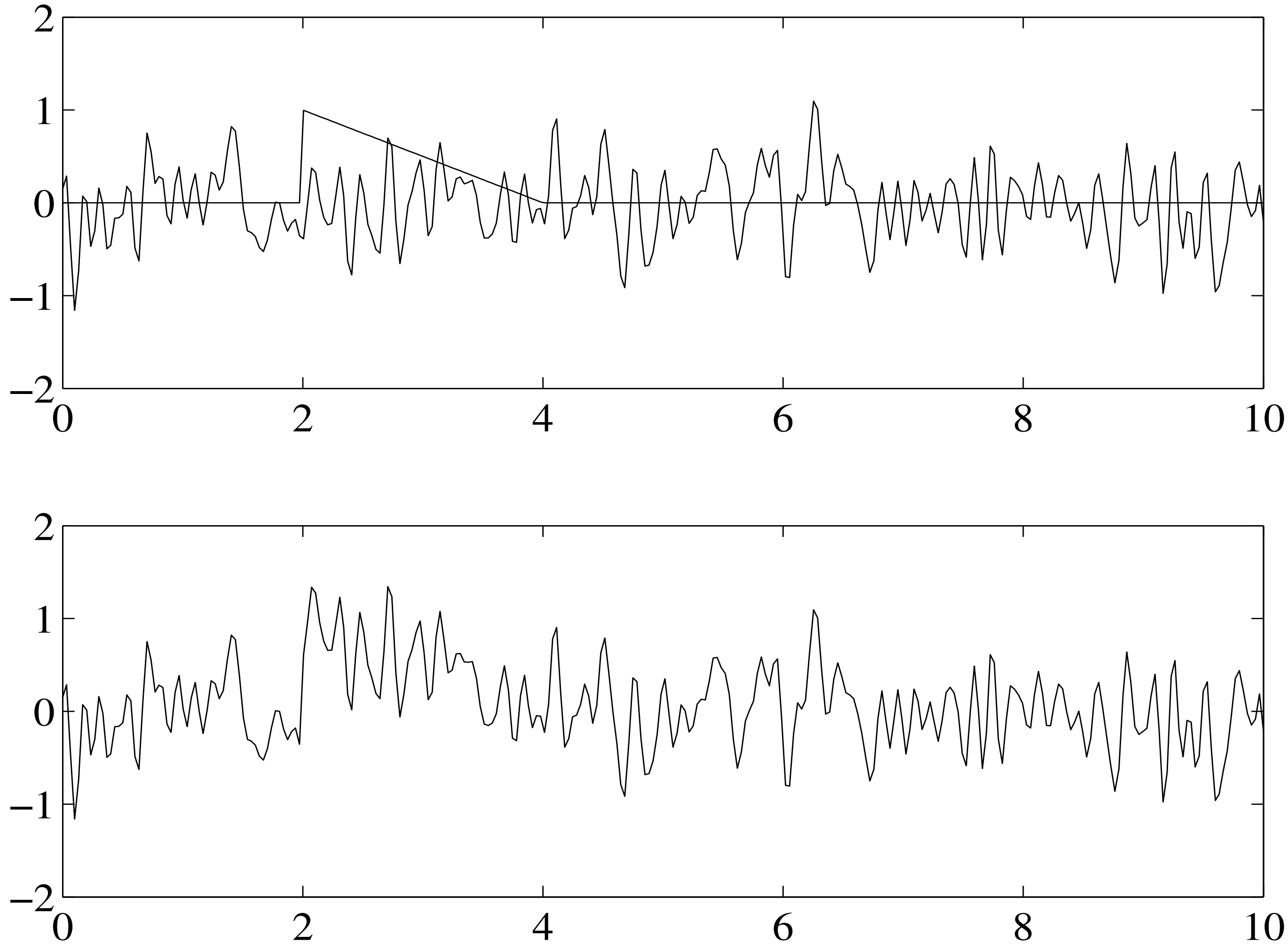

***Figure* 10.21.** A triangular signal $v(t)$ and broadband noise X_t (top). Their sum, $v(t) + X_t$ (bottom), shows that the noise hides the presence of the signal.

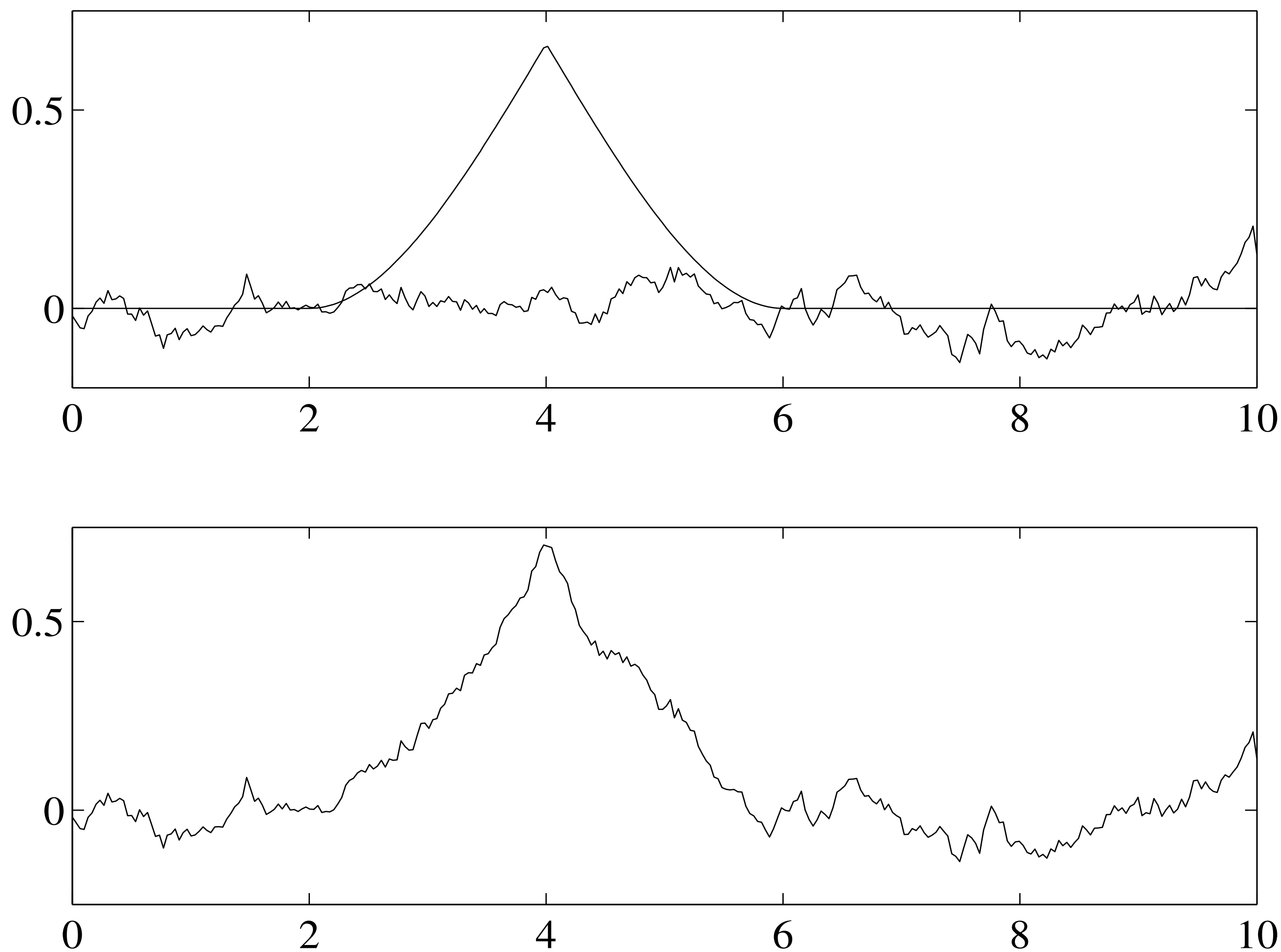

***Figure* 10.23.** Matched filter output terms $v_o(t)$ and Y_t (top) and their sum $v_o(t) + Y_t$ (bottom), when $v(t)$ is the signal at the top in Figure 10.19 and $H(f)$ is the corresponding matched filter.

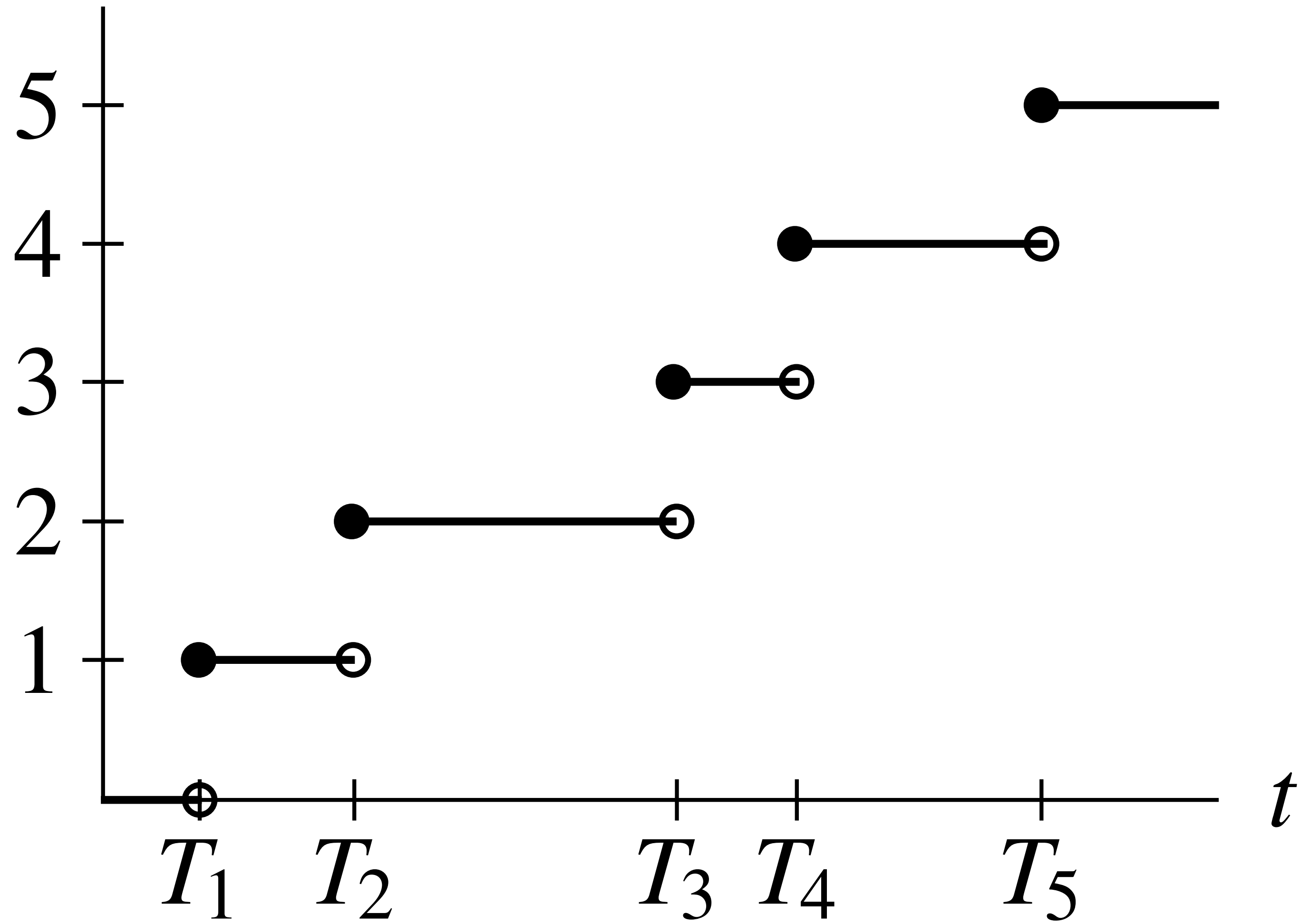

***Figure* 11.1.** Sample path N_t of a counting process.

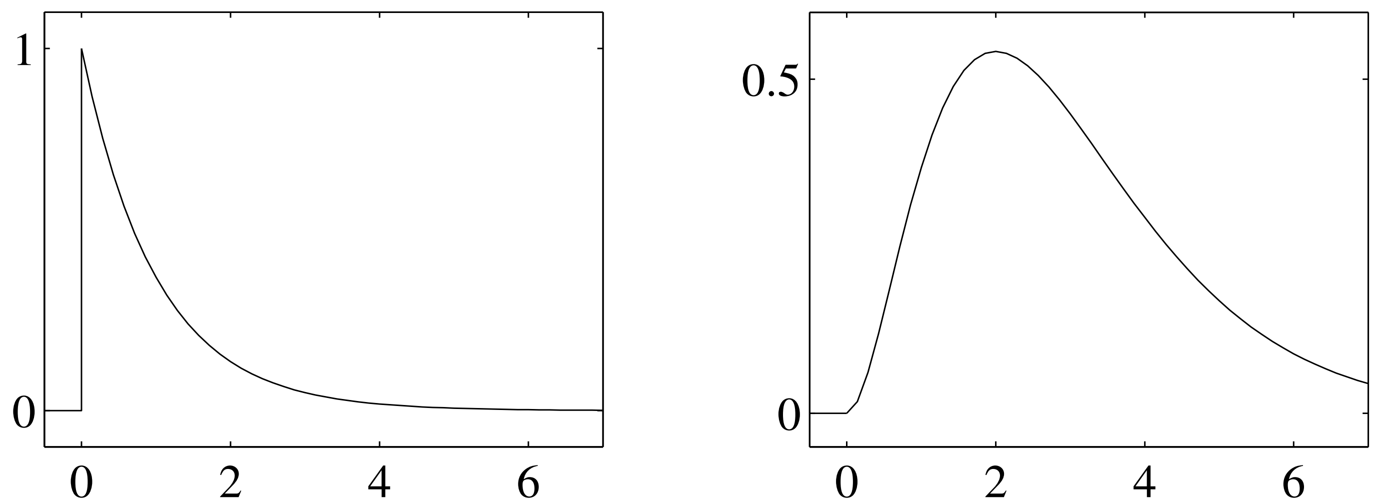

***Figure* 11.2.** Plots of $h(t) = e^{-t}u(t)$ (left) and $h(t) = t^2e^{-t}u(t)$ (right), where $u(t)$ is the unit step function.

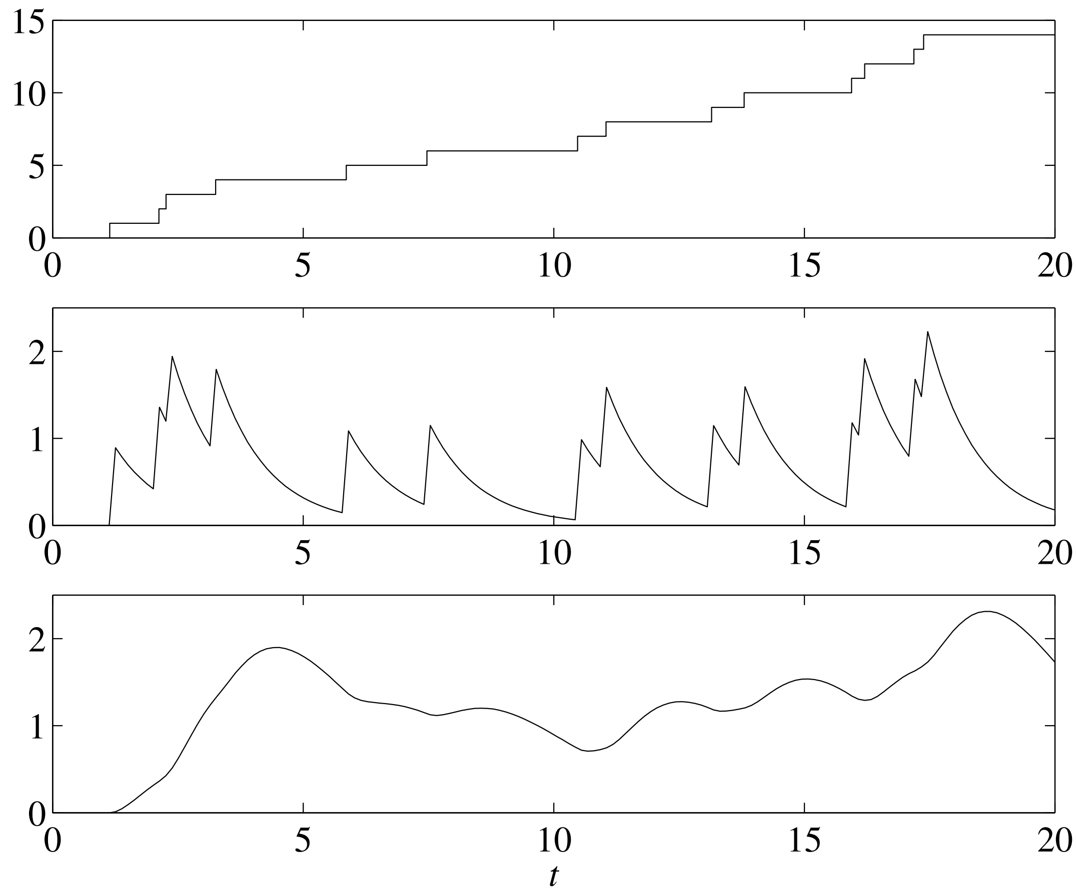

***Figure* 11.3.** Point process N_t (top) and corresponding shot noise Y_t in Eq. (11.8) for $h(t) = e^{-t}u(t)$ (middle) and for $h(t) = t^2e^{-t}u(t)$ (bottom), where $u(t)$ is the unit step function.

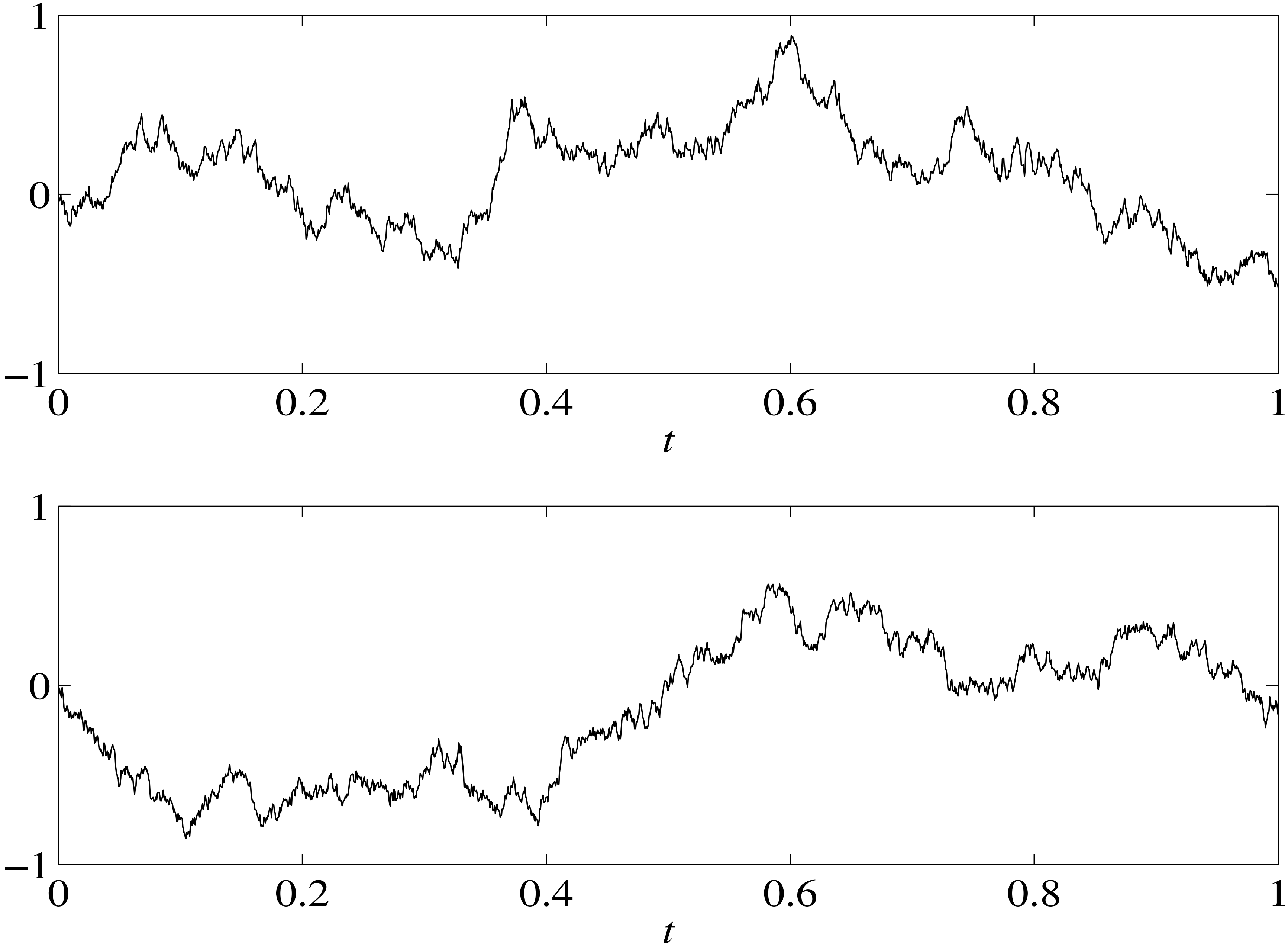

***Figure* 11.4.** Two sample paths of a standard Wiener process.

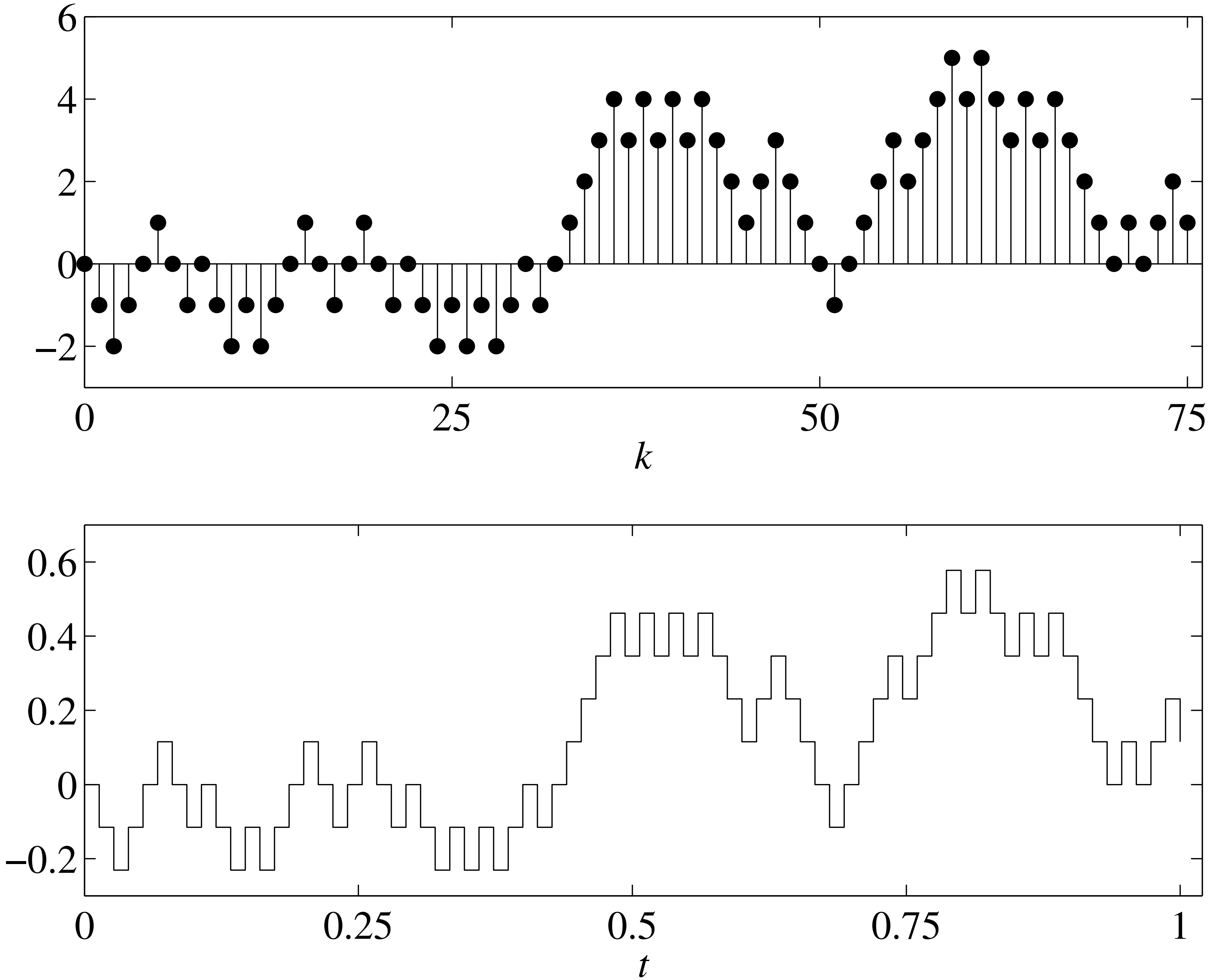

Figure **11.5.** Sample path $S_k, k = 0, \ldots, 75$ (top). Sample path $W_t^{(75)}$ (bottom).

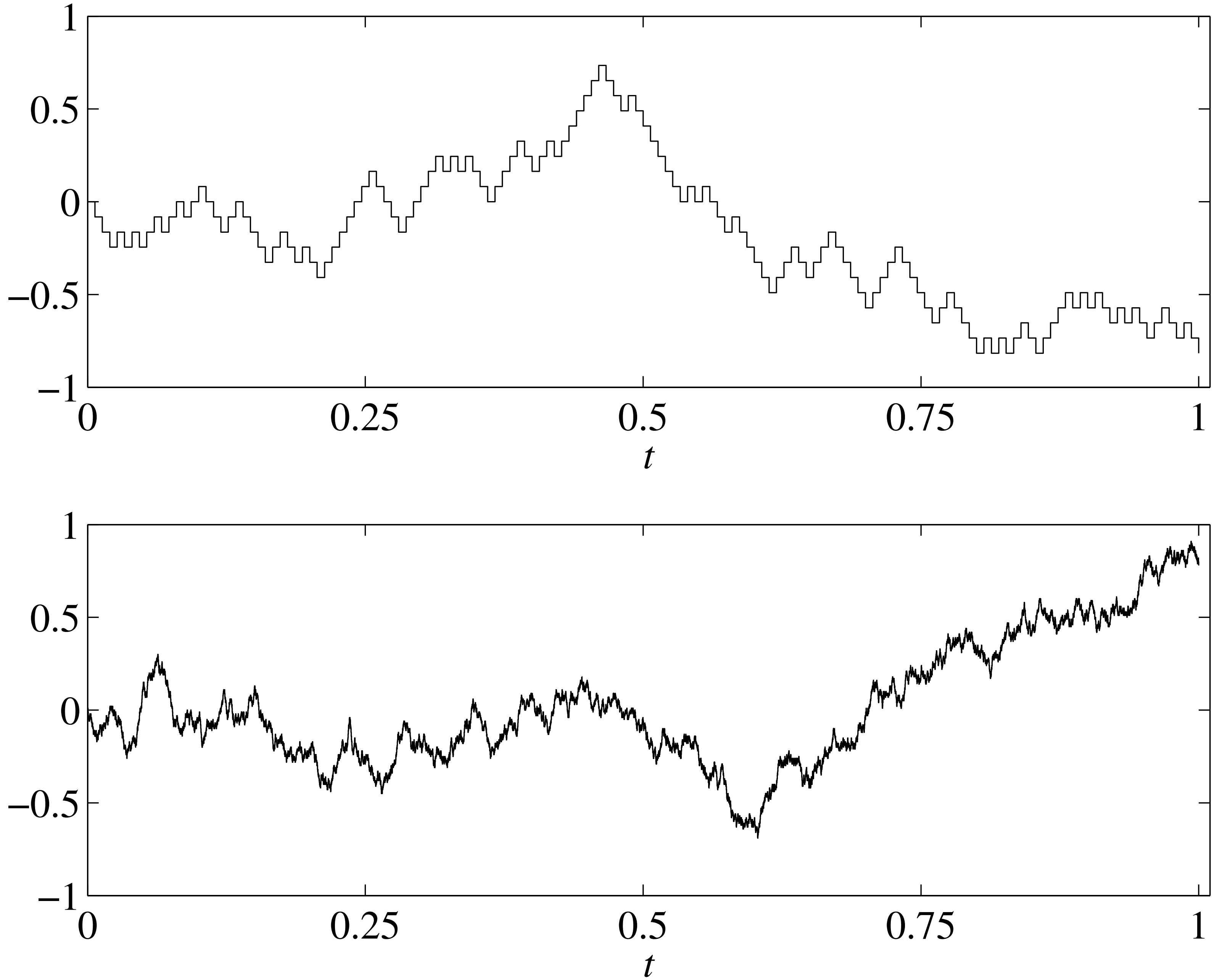

***Figure* 11.6.** Sample path of $W_t^{(n)}$ for $n = 150$ (top) and for $n = 10000$ (bottom).

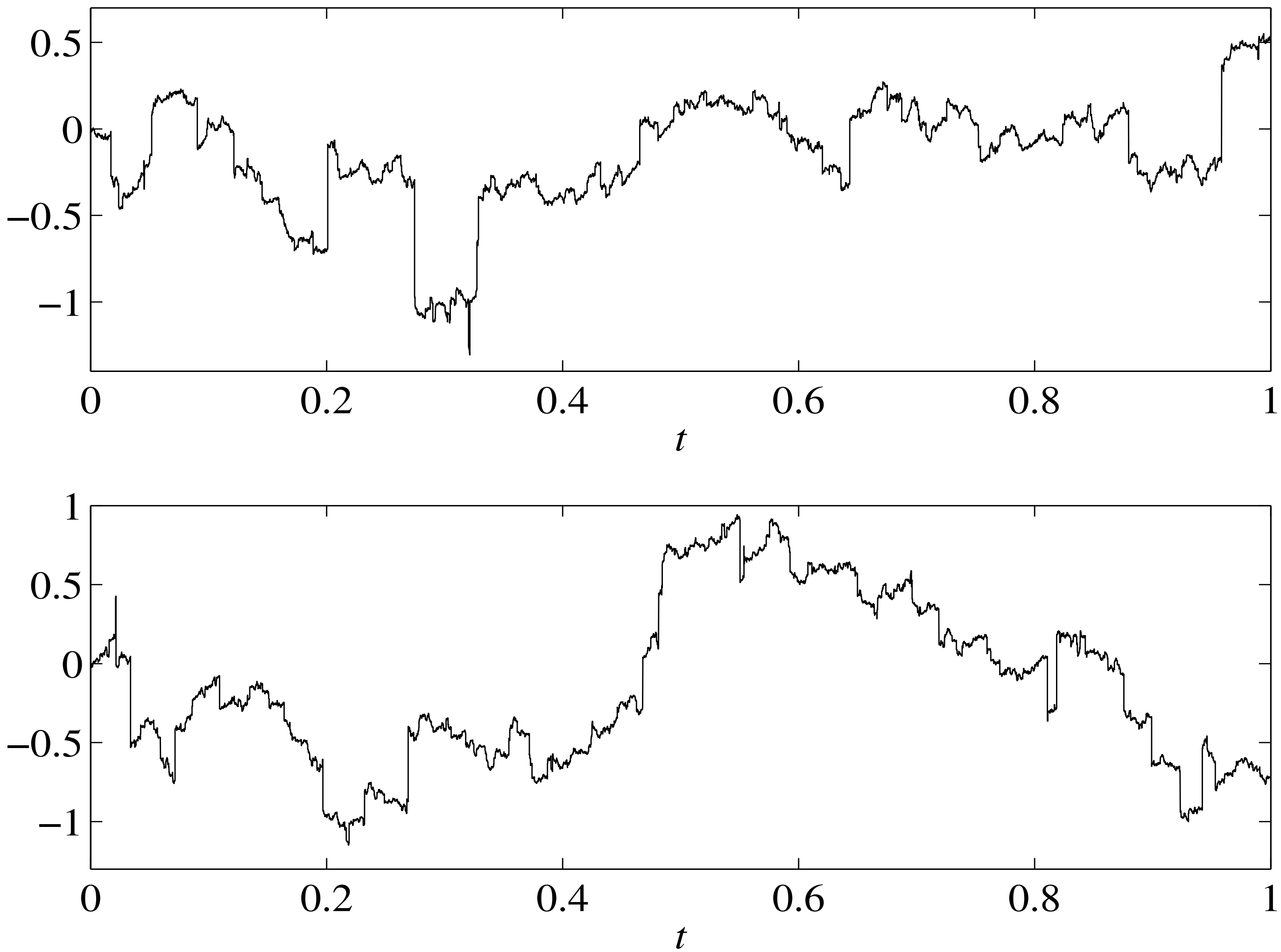

***Figure* 11.7.** Two sample paths of $S_{\lfloor nt \rfloor}/n^{2/3}$ for $n = 10\,000$ when the X_i have Student's t density with $3/2$ degrees of freedom.

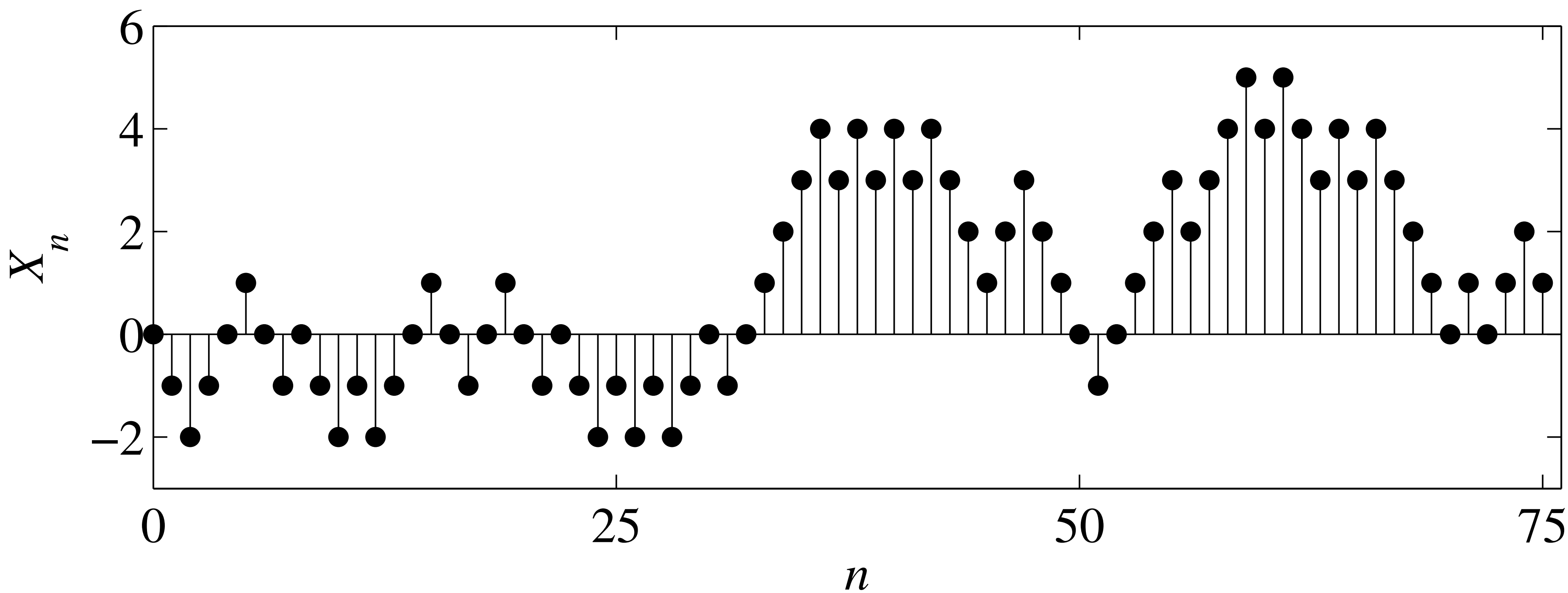

***Figure* 12.1.** Realization of a symmetric random walk X_n.

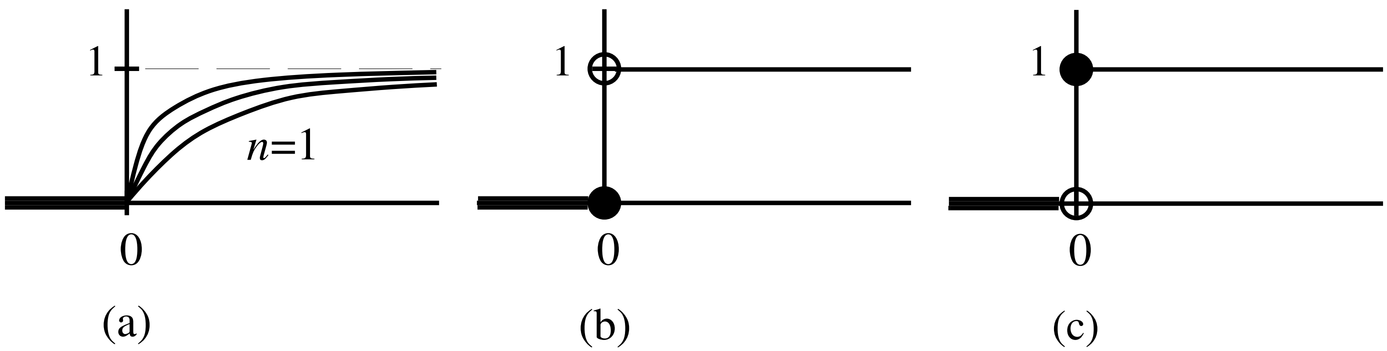

***Figure* 14.2.** (a) Sketch of $F_{X_n}(x)$ for increasing values of n. (b) Pointwise limit of $F_{X_n}(x)$. (c) Limiting cdf $F_X(x)$.

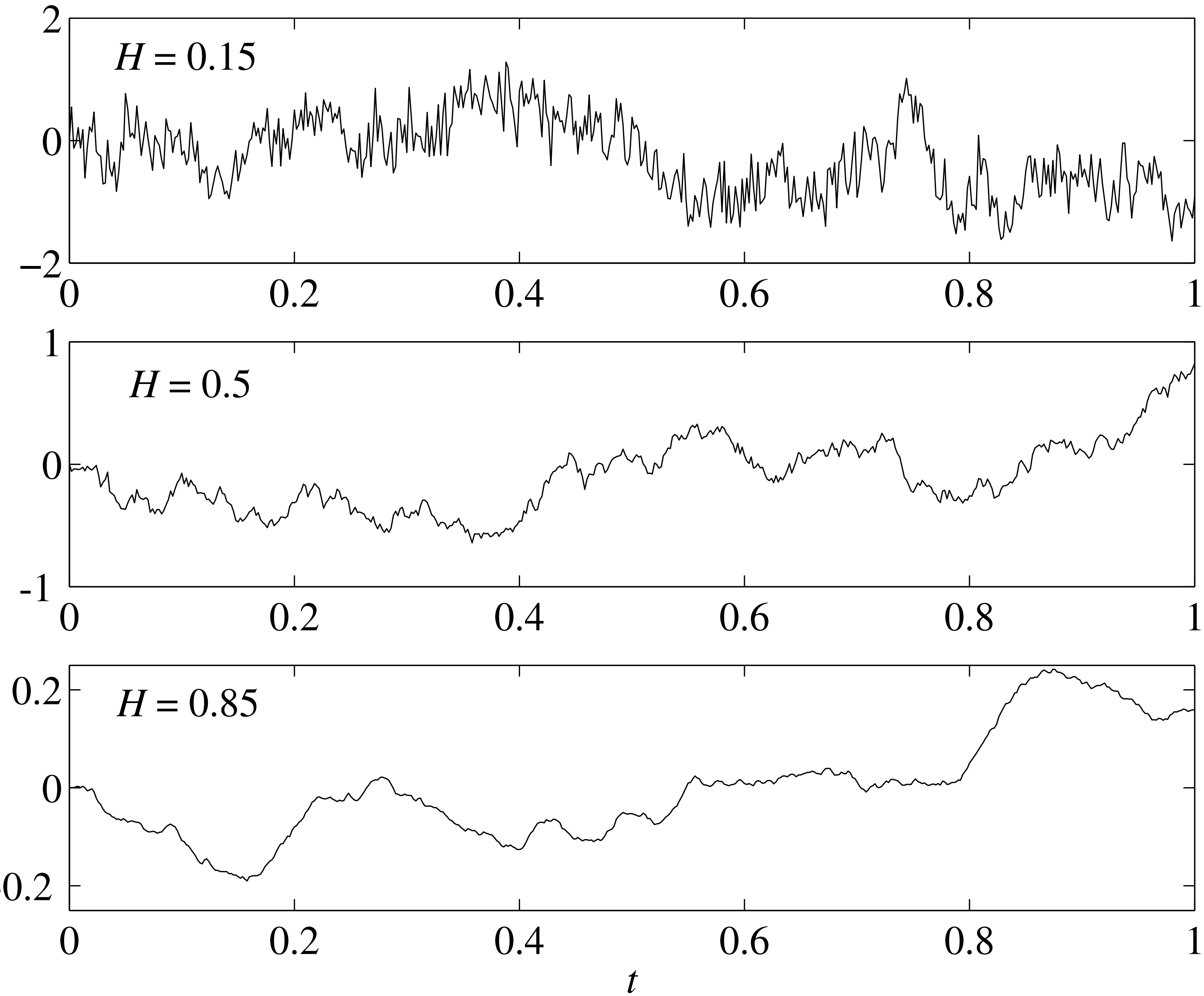

***Figure* 15.1.** Fractional Brownian motions with $H = 0.15$, $H = 0.5$, and $H = 0.85$.